Title
Investigating novel roles and regulation of SPRED proteins in MAPK signaling

Author
Lopez, Jocelyne

Publication Date
2023

Peer reviewed|Thesis/dissertation

Investigating novel roles and regulation of SPRED proteins in MAPK signaling

by
Jocelyne Lopez

DISSERTATION
Submitted in partial satisfaction of the requirements for degree of
DOCTOR OF PHILOSOPHY

in

Biochemistry and Molecular Biology

in the

GRADUATE DIVISION
of the
UNIVERSITY OF CALIFORNIA, SAN FRANCISCO

Approved:

DocuSigned by:
Natalia Jura
E438674A382B42F...

Natalia Jura
Chair

DocuSigned by:
Frank Mccormick
DocuSigned by:
Davide Ruggero
14C3B6AD60C5446...

Frank Mccormick

Davide Ruggero

Committee Members

Para mis queridos padres, Petra y Felipe. And to my sister, Dawn.

Acknowledgements

My journey through graduate school would not have been possible without the support of numerous mentors and encouragement from my loved ones. I am deeply grateful for the unwavering support I've received throughout my academic journey, and I hope to highlight a few of those key individuals here.

I thank my thesis advisor, Dr. Frank McCormick, for his exceptional mentorship, unwavering support, and countless opportunities that have propelled my career forward. Frank, I am deeply grateful for your belief in my abilities and your enthusiasm for science, which have been a constant source of inspiration throughout my journey. Your expertise, guidance, and constructive feedback have helped me to overcome challenges, realize my potential, and develop my skills as a scientist. Over the past four years, I have had the privilege of working with the coolest boss ever, and I feel honored to have learned from the most brilliant scientist in the field.

I would like to thank to my thesis committee, Dr. Davide Ruggero and Dr. Natalia Jura, for their invaluable support and insightful scientific discussions.

I also thank members of the McCormick lab. You all have helped me progress into the scientist I am today. Thank you all for all the memories, laughs, and valuable lessons. I thank Dr. Andrew Wolfe for being my rotation mentor and making my introduction into the McCormick lab so welcoming. I thank Dr. Lucy Young and Dr. Matthew Sale for their support, scientific discussions, and for providing me the tools to progress my project. I would also like to extend my appreciation to Dr. Pau Castel for serving as my mentor throughout my PhD journey. Pau, thank you for your support, guidance, and motivation that have been pivotal in shaping my academic and personal growth. Your valuable insights, constructive feedback, and rigorous challenges have helped me to develop my project and hone my research skills. Thank you for being an outstanding mentor and

for inspiring me to achieve my fullest potential. I also thank Dr. Antonio Cuevas, Armando Martinez, and Richard Van for their friendship, guidance, and support.

I have immense gratitude towards Dr. D'Anne Duncan and her team. D'Anne, thank you for fostering community for me.

I cannot imagine going through my graduate career without all the friends I've made along the way. I especially would like to thank Evelyn Hernandez, Natasha Puri, Harold Marin, Yewande Alabi, Hayden Saunders, and Priscilla Munoz. You all have been then there for me in so many ways and I cannot express how thankful I am that we got to go through grad school together. Additionally, I am grateful for my partner, Gustavo. Thank you for encouraging and motivating me, especially during the challenging final stretches of my PhD when I thought I could never finish.

I thank the many mentors I gained while at UC Irvine that supported me in my journey to graduate school. I thank Dr. Manuela Raffatellu for granting me my first ever research opportunity and to Dr. Vladimir Ochoa for taking me in under his wing. From teaching me how to pipette to teaching me how to think about experiments, I'm not sure I would have ever known about research had it not been for you, Vlad. I greatly thank Dr. Claudia Benavente and members of the Benavente lab. My time in the Benavente lab was so special and I'm so thankful for all the mentorship Claudia has offered me, even past my undergraduate studies. Thank you for always making your lab feel so inclusive and for giving me the support, inspiration, and confidence to be a scientist.

Lastly, I would like to thank my family for their endless support throughout all my education. I thank my mom and dad for all the sacrifices they made so I could have more opportunities in life and for always encouraging and believing in me. While there may have been times when you wished you could have helped or guided me with my studies, you both raised me to be equipped

with the essential skills and values that have enabled me to be successful. I thank all my grandparents, aunts, uncles, cousins, nephew, (soon to come niece), and brother-in-law. My family has always been my greatest cheerleaders and you all know how to ground me, especially during my times of stress. I owe a huge thank my sister, Dawn, who has always been my best friend and greatest supporter. Sister, you've been through it all with me; thank you for always listening to me during times of difficulty and for your words of encouragement. You've always believed in me, more than I ever believed in myself. I could not have done it without you.

Contributions

Chapter 2 is adapted from a manuscript published in *JBC*, by the following authors: **Jocelyne Lopez**, Daniel A. Bonsor, Matthew J. Sale, Anatoly Urisman, Jennifer L. Mehalko, Miranda Cabanski-Dunning, Pau Castel, Dhirendra K. Simanshu, Frank McCormick.

Jocelyne Lopez: Conceptualization, Writing - Original Draft, Investigation. Daniel A. Bonsor: Investigation, formal analysis, Writing- Reviewing and Editing. Matthew J. Sale: Writing- Reviewing and Editing, Methodology, Resources. Anatoly Urisman: Investigation, formal analysis, Writing- Reviewing and Editing. Jennifer L. Mehalko: Investigation. Miranda Cabanski-Dunning: Investigation. Pau Castel: Writing- Reviewing and Editing, Conceptualization, Methodology. Dhirendra K. Simanshu: Investigation, formal analysis, Writing- Reviewing and Editing. Frank McCormick: Writing- Reviewing and Editing, Supervision, Conceptualization.

Chapter 3 is adapted from an unpublished manuscript by the following authors, by the following authors: **Jocelyne Lopez**, Juan Antonio Camara Serrano, Pau Castel, Frank McCormick.

Jocelyne Lopez: Conceptualization, Writing - Original Draft, Investigation. Juan Antonio Camara Serrano: Investigation, formal analysis. Pau Castel: Writing- Reviewing and Editing, Conceptualization. Frank McCormick: Writing- Reviewing and Editing, Supervision, Conceptualization.

Investigating novel roles and regulation of SPRED proteins in MAPK signaling

Jocelyne Lopez

Abstract

Sprouty-related EVH-1 domain-containing (SPRED) proteins are a family of proteins that negatively regulate the RAS-MAPK pathway, which is involved in the regulation of the mitogenic response and cell proliferation. However, the mechanism by which these proteins affect RAS-MAPK signaling has not been fully elucidated. Patients with mutations in SPRED give rise to unique disease phenotypes, thus we hypothesized that distinct interactions across SPRED proteins may account for alternative nodes of regulation. Chapter 2 shows our efforts to characterize the SPRED interactome and evaluate how members of the SPRED family function through unique binding partners, here we performed affinity purification mass spectrometry. We identified 90-kDa ribosomal S6 kinase 2 (RSK2) as a specific interactor of SPRED2, but not SPRED1 or SPRED3. We identified that the N-terminal kinase domain of RSK2 mediates interaction between amino acids 123-201 of SPRED2. Using X-ray crystallography, we determined the structure of the SPRED2-RSK2 complex and identified the SPRED2 motif, F145A, as critical for interaction. Additionally, we found that formation of this interaction is regulated by MAPK signaling events. We also find that that this interaction between SPRED2 and RSK2 has functional consequences, whereby knockdown of SPRED2 resulted in increased phosphorylation of RSK substrates, YB1 and CREB. Furthermore, SPRED2 knockdown hindered phospho-RSK membrane and nuclear subcellular localization. Lastly, we report that disruption of the SPRED2-RSK complex has effects on RAS-MAPK signaling dynamics. Overall, our analysis reveals that members of the SPRED

family have unique protein binding partners and describes the molecular and functional determinants of SPRED2-RSK2 complex dynamics.

Model organism are important tools to investigate molecular mechanisms in vivo. In effort to evaluate the molecular mechanisms of SPRED2 in vivo, we set out to use a previously published SPRED2 mouse models. However, when undergoing studies, we observed several discrepancies in the mice phenotypes. Chapter 3 is a letter to editor, in response to the discrepancies we observed in these mice.

Table of Contents

List of Figures

List of Tables

Chapter 1: Introduction

Negative regulation of the RAS- MAPK pathway

Mitogenic signaling mediated by Receptor Tyrosine Kinases (RTKs) plays important roles in regulating various cellular processes such as proliferation and differentiation (1, 2). It is essential that these events are regulated, otherwise over activation of these signals results in hyperproliferation or inhibition of proper cellular maturation during development. Accordingly, these signals are typically stringently regulated by various negative feedback loops that coordinate signaling events following RTK activation (2). For instance, activated ERK1/2 initiates these negative feedback loops by inducing the expression of various negative regulators of the Mitogen-Activated Protein Kinase (MAPK) pathway, including Sprouty-related protein with EVH-1 domain (SPRED) (3).

SPRED proteins and mechanism

The SPRED family of proteins consists of SPRED1, SPRED2, and SPRED3; each containing an N-terminal Ena/Vasp Homology (EVH-1) domain that mediates protein-protein interactions, a c-KIT binding domain (KBD) mediating interaction with Receptor Tyrosine Kinases (RTKs), and a C-terminal sprouty related (SPR) domain important for membrane localization (**Fig. 1.1A**) (4, 5). A key function of SPRED1 is to bind and transport the RAS-GTPase Activating Protein (GAP), Neurofibromin, from the cytosol to the membrane where Neurofibromin negatively regulates the RAS pathway by hydrolyzing active RAS.GTP to the inactive RAS.GDP state (6). While SPRED proteins are generalized as negative regulators of MAPK signaling, it remained unclear how members of the SPRED family function or how they are regulated at the protein level to fine tune mitogenic signaling for proper cellular differentiation

and development. Chapter 2 explores this further, detailing the identification and characterization the specific interaction between SPRED2 and RSK2.

SPRED and RSK2 in disease

While SPREDs do not have catalytic activity, they can interact with the RAS GTPase activating protein (GAP), Neurofibromin, and localize it the plasma membrane where it can be in proximity to hydrolyze RAS.GTP to the inactive RAS.GDP state (6). Germline loss-of-function mutations in *SPRED1* that disrupt interaction with Neurofibromin cause the Rasopathy, Legius syndrome (7). This disease is characterized by hyperactivation of the RAS-MAPK pathway and patients have varying developmental abnormalities such as café-au-lait spots and behavioral problems (8).

Similar to SPRED1, SPRED2 also interacts with the RAS GAP, Neurofibromin, through the same residues in the EVH-1 domain (6, 7, 9, 10). Recently, studies have identified *SPRED2* loss of function mutations in patients with the Rasopathy, Noonan Syndrome (11). These mutations also hinder interaction with Neurofibromin, resulting in hyperactive RAS signaling. These patients develop distinct phenotypes including skeletal abnormalities and heart defects.

In chapter 2, we characterize the SPRED2 interactome and identify a unique interaction between SPRED2 and the Ribosomal S6 Kinase 2 (RSK2). RSK2 is a serine/threonine kinase that acts as a key effector of the RAS-MAPK pathway to regulate several biological functions such as cell cycle progression, transcription, and apoptosis (12). Moreover, RSK2 targets key substrates during development; thus, germline loss-of-function mutations in *RPS6KA3*, the gene encoding RSK2, causes Coffin-Lowry syndrome, a syndrome characterized by mental retardation, skeletal anomalies, and cardiac defects (13–15). Interestingly, *RPS6KA3* and *SPRED2* loss of function mutations share similar skeletal and cardiac defect phenotypes, providing a genetic link between

the biochemical interaction identified. Chapter 2 outlines the biochemical and functional characterization of this interaction and provides a suggested model for how disruption of this complex results in hyperactive signaling and could contribute to the pathogenesis of these developmental disorders.

SPRED mouse models

Several *Spred* knockout (KO) models have been developed to better understand their involvement in various diseases. The *Spred1* KO mice show signs of cognitive impairment and have shortened faces, which is similar to Legius syndrome in humans (16). Previous studies have suggested that the *Spred2* KO mice have an achondroplasia-like phenotype, which is a developmental disorder that manifests as short stature and craniofacial abnormalities (17). Additionally, the *Spred2* KO mice exhibit growth retardation and cardiac hypertrophy, resembling the Noonan syndrome-like phenotype(11) . However, our work outlines discrepancies in these previously reported in *Spred2* KO mice phenotypes, as detailed in chapter 3.

Furthermore, it has been observed that double knock out *Spred1* and *Spred2* mice are embryonic lethal suggesting redundancy between SPRED1 and SPRED2 (18). However, as described in chapter 2, unique protein interactors have been identified for each SPRED protein, indicating that they may have distinct mechanisms of action.

References:

1. Roovers, K., and Assoian, R. K. (2000) Integrating the MAP kinase signal into the G1 phase cell cycle machinery. *Bioessays*. 22, 818–826

2. Neben, C. L., Lo, M., Jura, N., and Klein, O. D. (2019) Feedback regulation of RTK signaling in development. *Dev Biol*. 447, 71–89

3. Xie, Y., Cao, Z., Wong, E. W. P., Guan, Y., Ma, W., Zhang, J. Q., Walczak, E. G., Murphy, D., Ran, L., Sirota, I., Wang, S., Shukla, S., Gao, D., Knott, S. R. V., Chang, K., Leu, J., Wongvipat, J., Antonescu, C. R., Hannon, G., Chi, P., and Chen, Y. (2018) COP1/DET1/ETS axis regulates ERK transcriptome and sensitivity to MAPK inhibitors. *J Clin Invest*. 128, 1442–1457

4. Wakioka, T., Sasaki, A., Kato, R., Shouda, T., Matsumoto, A., Miyoshi, K., Tsuneoka, M., Komiya, S., Baron, R., and Yoshimura, A. (2001) Spred is a Sprouty-related suppressor of Ras signalling. *Nature*. 412, 647–651

5. Kato, R., Nonami, A., Taketomi, T., Wakioka, T., Kuroiwa, A., Matsuda, Y., and Yoshimura, A. (2003) Molecular cloning of mammalian Spred-3 which suppresses tyrosine kinase-mediated Erk activation. *Biochem Bioph Res Co*. 302, 767–772

6. Stowe, I. B., Mercado, E. L., Stowe, T. R., Bell, E. L., Oses-Prieto, J. A., Hernández, H., Burlingame, A. L., and McCormick, F. (2012) A shared molecular mechanism underlies the human rasopathies Legius syndrome and Neurofibromatosis-1. *Gene Dev*. 26, 1421–1426

7. Brems, H., Chmara, M., Sahbatou, M., Denayer, E., Taniguchi, K., Kato, R., Somers, R., Messiaen, L., Schepper, S. D., Fryns, J.-P., Cools, J., Marynen, P., Thomas, G., Yoshimura, A., and Legius, E. (2007) Germline loss-of-function mutations in SPRED1 cause a neurofibromatosis 1–like phenotype. *Nat Genet*. 39, 1120–1126

8. Rauen, K. A. (2013) The RASopathies. *Annu Rev Genom Hum G*. 14, 355–369

9. Kolanczyk, M., and Stevenson, D. A. (2015) Molecular Genetics of Pediatric Orthopaedic Disorders. 10.1007/978-1-4939-2169-0_2

10. Dunzendorfer-Matt, T., Mercado, E. L., Maly, K., McCormick, F., and Scheffzek, K. (2016) The neurofibromin recruitment factor Spred1 binds to the GAP related domain without affecting Ras inactivation. *Proc National Acad Sci*. 113, 7497–7502

11. Motta, M., Fasano, G., Gredy, S., Brinkmann, J., Bonnard, A. A., Simsek-Kiper, P. O., Gulec, E. Y., Essaddam, L., Utine, G. E., Prandi, I. G., Venditti, M., Pantaleoni, F., Radio, F. C., Ciolfi, A., Petrini, S., Consoli, F., Vignal, C., Hepbasli, D., Ullrich, M., Boer, E. de, Vissers, L. E. L. M., Gritli, S., Rossi, C., Luca, A. D., Becher, S. B., Gelb, B. D., Dallapiccola, B., Lauri, A., Chillemi, G., Schuh, K., Cavé, H., Zenker, M., and Tartaglia, M. (2021) SPRED2 loss-of-function causes a recessive Noonan syndrome-like phenotype. *Am J Hum Genetics*. 108, 2112–2129

12. Anjum, R., and Blenis, J. (2008) The RSK family of kinases: emerging roles in cellular signalling. *Nat Rev Mol Cell Bio*. 9, 747–758

13. Yang, X., Matsuda, K., Bialek, P., Jacquot, S., Masuoka, H. C., Schinke, T., Li, L., Brancorsini, S., Sassone-Corsi, P., Townes, T. M., Hanauer, A., and Karsenty, G. (2004) ATF4 Is a Substrate of RSK2 and an Essential Regulator of Osteoblast Biology. *Cell*. 117, 387–398

14. Hanauer, A., and Young, I. D. (2002) Coffin-Lowry syndrome: clinical and molecular features. *J Med Genet*. 39, 705–713

15. Pereira, P. M., Schneider, A., Pannetier, S., Heron, D., and Hanauer, A. (2009) Coffin–Lowry syndrome. *Eur J Hum Genet*. 18, 627–633

16. Inoue, H., Kato, R., Fukuyama, S., Nonami, A., Taniguchi, K., Matsumoto, K., Nakano, T., Tsuda, M., Matsumura, M., Kubo, M., Ishikawa, F., Moon, B., Takatsu, K., Nakanishi, Y., and Yoshimura, A. (2005) Spred-1 negatively regulates allergen-induced airway eosinophilia and hyperresponsiveness. *J Exp Medicine*. 201, 73–82

17. Bundschu, K., Knobeloch, K.-P., Ullrich, M., Schinke, T., Amling, M., Engelhardt, C. M., Renné, T., Walter, U., and Schuh, K. (2005) Gene Disruption of Spred-2 Causes Dwarfism*. *J Biol Chem*. 280, 28572–28580

18. Taniguchi, K., Kohno, R., Ayada, T., Kato, R., Ichiyama, K., Morisada, T., Oike, Y., Yonemitsu, Y., Maehara, Y., and Yoshimura, A. (2007) Spreds Are Essential for Embryonic Lymphangiogenesis by Regulating Vascular Endothelial Growth Factor Receptor 3 Signaling. *Mol Cell Biol*. 27, 4541–4550

Chapter 2: The Ribosomal S6 Kinase 2 (RSK2)-SPRED2 complex regulates phosphorylation of RSK substrates and MAPK signaling

Mitogenic signaling mediated by Receptor Tyrosine Kinases (RTKs) activates the RAS- Mitogen-Activated Protein Kinase (MAPK) pathway to regulate various cellular processes such as proliferation and differentiation (1, 2). Hyperactivation of this pathway is known to drive many diseases, including cancer, and is also the underlying cause of a group of developmental disorders collectively termed RASopathies (3, 4). Given the importance of this pathway for cellular homeostasis, these mitogenic signals are stringently regulated at different levels of the pathway by various negative feedback and feedforward loops that coordinate signaling events following RTK activation (2). Sprouty-related protein with EVH-1 domain (SPRED) are a family of proteins that negatively regulate the RAS-MAPK pathway (5). This family consists of SPRED1, SPRED2, and SPRED3, each containing an N- terminal Ena/Vasp Homology (EVH-1) domain, a c-KIT binding domain (KBD), a C-terminal sprouty related (SPR) domain, and two uncharacterized domains (**Fig. 2.1A**) (5, 6). Although SPREDs do not exhibit any enzymatic activity, they can regulate RAS-MAPK signaling, mainly through a direct interaction between their EVH-1 domain binding to the RAS-GTPase Activating Protein (GAP), neurofibromin. This interaction localizes neurofibromin to the plasma membrane, which catalyzes RAS GTPase activity and inactivates the cascade (7–9). Germline loss-of-function variants in *SPRED1* cause Legius syndrome, a RASopathy characterized by varying developmental abnormalities such as *café-au-lait* skin spots and behavioral traits (10). Although *SPRED2* or *SPRED3* pathogenic variants are not found in individuals with Legius syndrome, a recent study has observed *SPRED2* loss-of-function variants in individuals with Noonan syndrome, another RASopathy caused by hyperactivation of the RAS-MAPK pathway (11). Furthermore, *Spred1* knockout (KO) mice exhibit a phenotype that

resembles Legius syndrome characterized by shortened faces and learning disabilities (12, 13). In contrast, *Spred2* KO mice show discrepancies in their reported phenotypes; while initial studies did not describe any significant phenotypes in these mice, another group has recently proposed that these mice exhibit a Noonan syndrome-like phenotype (11, 14) . Despite these inconsistencies, there is a clear phenotypic difference between *Spred1* and *Spred2* null mice, suggesting unique functions for these genes that have yet to be identified (15). We reasoned that unique protein interactions across SPRED proteins may account for their specific phenotypes and functions. Here, we used a systematic approach to characterize the interactome of SPRED proteins and identify unique protein binding partners that may contribute to their distinct roles. Using affinity purification mass spectrometry, we identified an interaction between SPRED2, but not SPRED1 or SPRED3, and serine/threonine kinase ribosomal protein s6 kinase alpha-2 (RSK2). We further characterized the biochemical and structural properties of this interaction and describe a potential mechanism of the SPRED2-RSK2 complex in regulating the RAS-MAPK signaling pathway.

RESULTS

A proteomic screen reveals common and unique interactors of SPRED proteins

To identify potential binding partners of the SPRED family, we performed affinity purification-mass spectrometry of FLAG-tagged SPRED proteins expressed in cultured cells. Neurofibromin was a top common interactor across all SPRED proteins, as previously reported (**Fig. 2.1B**) (7). In addition, we identified RSK2 and 14-3-3 proteins as unique interactors of SPRED2 and SPRED3, respectively (**Fig. S2.1A**). The results from our proteomics screening were validated by immunoprecipitation of the individual SPRED proteins from cell extracts and immunoblotting of endogenous proteins (**Figs. 2.1C and S2.1B**). 14-3-3 proteins are a family of proteins that bind to

phospho-serine and phospho-threonine recognition motifs to function as molecular scaffolds, regulate protein function, or alter protein localization (16). RSK2 is a serine/threonine kinase that acts as downstream effector of the RAS-MAPK pathway to regulate cell cycle progression, transcription, and apoptosis (17). Given the connection with the RAS-MAPK pathway, we focused on the SPRED2-RSK2 interaction for further characterization.

Identification of a unique SPRED2 domain that mediates RSK2 interaction

To evaluate the motifs that mediate interaction between SPRED2 and RSK2, we performed binding assays using a series of SPRED2 truncation mutants (**Figs. 2.2A and S2.2A**). We identified amino acids 123-200 as necessary and sufficient for interaction with RSK2 (**Fig. 2.2B**). These amino acids encompass a domain of SPRED2 that does not exhibit sequence homology with other family members (**Fig. 2.1A**). To further confirm the role of this domain in RSK2 interaction, we generated chimeric proteins in which the SPRED2 amino acids 123-200 were replaced with the corresponding amino acids in SPRED1 and SPRED3, and tested binding to RSK2. Using these proteins, we found RSK2 binding to SPRED1 and SPRED3 chimeras (**Fig. 2.2C**). We refer to this motif as the RSK interacting domain (RID), however it is unknown whether SPRED2 may have additional protein interactors in this region (**Fig. 2.2A**).

RSK kinases phosphorylate SPRED2

RSK kinases contain an N-terminal kinase domain (NTKD) and a C-terminal kinase domain (CTKD) that are activated through a cascade of phosphorylation events mediated by upstream ERK1/2 and PDK1 kinases (**Fig. 2.3A**) (17) . The RSK family consists of RSK1-4, and they have greater than 90% and 80% homology in their NTKD and CTKD domains, respectively (18). Using co-immunoprecipitation, we found that SPRED2 could interact with all four RSK family members (**Fig. 2.3B**). To identify the specific RSK2 domains that mediate interaction with SPRED2, we

generated truncations of RSK2 and found that SPRED2 interacted with the RSK2 NTKD (**Fig. 2.3C**). While RSK proteins have two kinase domains, only the NTKD is responsible for phosphorylating substrates (19). Hence, we speculated that SPRED2 might be a substrate of RSK kinases. RSK kinases phosphorylate substrates containing a consensus site that follows the motif RXX(S/T), where R is an Arginine, X is any amino acid, and (S/T) are phosphorylatable Serine or Threonine (20). We identified a putative RSK substrate consensus site (RXXS/T) within the SPRED2 protein sequence within amino acids 123-200, suggesting that SPRED2 may be phosphorylated by RSK2 at S167 and S168 (20). To evaluate the phosphorylation events on SPRED2 that may be mediated by RSK, we used HEK293 cells stably expressing the kinase domain of RAF1 (which is constitutively active) fused to the estrogen receptor (ER), henceforth referred as HR1 cells (**Fig. 2.3D**) (21, 22). When HR1 cells are treated with 4-hydroxytamoxifen (4-HT), the ligand binds ER, allowing for RAF1-mediated activation of canonical MAPK pathway, including downstream RSK kinases. Using this inducible model, we transiently transfected FLAG-tagged SPRED2 and assessed phosphorylation events through mass spectrometry when cells were treated with 4-HT to activate MAPK, or co-treated with an ERK1/2 inhibitor, pan-RSK inhibitor, or lambda phosphatase to remove all phosphorylation events. We identified two phosphorylation sites on SPRED2, S167 and S168, that were abrogated when cells were treated with a pan-RSK inhibitor (**Figs. 2.3E and S2.3A**). In support of our hypothesis, these sites reside on the putative RSK phosphorylation motif, RXXS/T, and are evolutionarily conserved in SPRED2 protein sequences (**Fig. 2.3F**). To validate these findings in vitro, we performed a kinase assay with recombinant RSK2 kinase domain and SPRED2 (104-297) proteins and assessed SPRED2 phosphorylation using a phospho-specific antibody that detects the RXX(S/T) motif. We detected ATP-dependent phosphorylation of SPRED2 (104-297) at RXXS/T sites, suggesting RSK can

directly phosphorylate SPRED2 and likely mediates the RSK-dependent phosphorylation of SPRED2 we observed in cells. (**Fig. 2.3G**). Furthermore, we found that mutating the S167/S168 phosphorylation sites to alanine, aspartic acid, or glutamic acid had no effect on SPRED2 binding to RSK2 or neurofibromin (**Fig. S2.4B**).

Structural analysis of SPRED2-RSK2 complex

To further characterize the SPRED2-RSK2 interaction, we used isothermal titration calorimetry (ITC) to measure the affinity of the interaction. We observed that the SPRED2 (104-181) protein bound the NTKD of RSK2 (44-367) with an affinity of approximately 9 μM (**Fig. S2.4A**). We synthesized additional peptides of various lengths and found the SPRED2 (140-151) and (138-153) peptides bound to the NTKD of RSK2, though with significantly weaker affinities of 36 and 20 μM, respectively (**Fig. S2.4A**). A slightly longer peptide, SPRED2 (131-160), bound the NTKD of RSK2 with similar thermodynamics and affinity to the SPRED2 (104-181) (**Fig. 2.4A**). Binding of SPRED2 (11-181), which includes the entirety of the EVH-1 domain, also bound with identical thermodynamics and affinity as SPRED2 (131-160) (**Fig. 2.4A**). This further suggests the complete SPRED2 RID is found within residues 131 to 160 (**Fig. 2.2B**). We used X-ray crystallography to solve the structure of the complex of the NTKD of RSK2 (46-346) in complex with SPRED2 RID (131-160). To obtain crystals of the complex, we used the pan-kinase inhibitor, quercitrin, to rigidify and stabilize the active site to achieve a final resolution of 1.8 Å. Despite using a 30-mer peptide, we only observed electron density for six residues of SPRED2 (^{141}DDDVFT^{146}) distal to the active site (**Fig. 2.4B**). These residues are bound within a cleft of RSK2, formed by two helices and a loop (residues 281-309), and residues 252, 259, 267 and 268. The SPRED2 hydrophobic residues, V144 and F145, were inserted within a hydrophobic pocket formed from the RSK2 residues W252, F259, F268, L285, G286, M287, F303 and R305. The acidic residues of RSK2

formed several hydrogen bonds to basic residues that line the RSK2 cleft (**Fig. S2.4B**). Specifically, SPRED2-D142 formed three hydrogen bonds to RSK2-R305, -N306 and -N307, whereas SPRED2-D143 forms a single hydrogen bond to RSK2-K304 (**Fig. 2.4C**). Two hydrogen bonds formed between SPRED2-T146 and RSK-R300 (**Fig. 2.4C**). Three additional hydrogen bonds formed between the main chain of SPRED2 (D141, D142 and V144) to RSK2 (**Fig. 2.4C**). In total nine hydrogen bonds formed at the interface and 940 $Å^2$ of RSK2 surface area was buried upon complex formation. The RSK2 binding pocket identified from our structural analysis is conserved across the RSK family, supporting our findings that SPRED2 can interact with the entire RSK family (**Fig. 2.3B and 2.4D**). Given that we only observed six residues of SPRED2 that interact with RSK2, we hypothesized that mutations at these sites would be critical for RSK2 binding. Accordingly, we found that the SPRED2 F145A mutant failed to pulldown RSK2, whereas the SPRED2 T146A mutant retained binding to RSK2 (**Fig. 2.4E**).

The MAPK pathway regulates SPRED2-RSK interaction

RSK activity is regulated by phosphorylation events that relieve auto-inhibition (17). Since ERK1/2 phosphorylation is a critical step for RSK activation, we assessed whether stimulation of the MAPK pathway could influence the SPRED2-RSK2 interaction. We transiently transfected FLAG-tagged SPRED2 into our inducible HR1 cells and observed that MAPK pathway activation strongly enhanced the interaction between SPRED2 and RSK1/ RSK2 (**Fig. 2.5A and S2.5A**). Additionally, we observed a significant band shift (corresponding to an increased apparent molecular weight in SDS-PAGE) in the species of RSK2 bound with SPRED2 compared to the flow-through of unbound RSK2. In co-immunoprecipitation experiments, we also found that SPRED2 interacted with the phosphorylated form of RSK2 (**Fig. S2.5B**). Together, these data suggest that post-translational modifications on RSK are required to enhance this interaction. To

test if phosphorylation of RSK2 by the upstream MAPK pathway would affect interaction with SPRED2, we treated cells with various MAPK inhibitors. Treatment with MEK1/2 or ERK1/2 inhibitors resulted in disruption of the SPRED2-RSK2 complex, whereas this interaction was unaffected by treatment with a RSK inhibitor (**Fig. 2.5B**). Additionally, treating lysates with lambda phosphatase to indiscriminately remove all phosphorylation events present in these lysates abolished the SPRED2-RSK2 interaction (**Figs. 2.5C and S2.5C**). Altogether, these data support a model in which MAPK signaling regulates the dynamics of the SPRED2-RSK complex.

SPRED2 regulates phosphorylation of RSK substrates and phospho-RSK membrane localization

A recent study has shown that RSK kinases bind to proteins containing a DDVF motif and that protein-protein interactions influence the phosphorylation of RSK substrates (23). Our biochemical and structural analyses also identified such a motif in SPRED2, and this prompted us to test whether the association with SPRED2 alters the phosphorylation of known RSK substrates. We overexpressed SPRED2 in cells and observed a decrease in the phosphorylation of the canonical RSK substrate, YB1 at S102 (**Figs. 2.6A and S2.6A**) (24). Similarly, we observed a decrease in RSK-mediated phosphorylation of Son of sevenless homolog 1 (SOS1) when SPRED2, but not when the RSK-binding deficient SPRED2 F145A mutant was overexpressed (**Fig. 2.6B**) (25). To further test these findings in an endogenous setting, we knocked down *SPRED2* in several cell lines (**Figs. 2.6C and S2.6B**). *SPRED2* knockdown resulted in an increase in phosphorylated CREB (S133) and phosphorylated YB1 (S102), further supporting a model whereby SPRED2 regulates RSK substrate availability. SPRED proteins are known to promote the membrane localization of neurofibromin and thus we hypothesized that SPRED2 may also regulate RSK localization. To test this, we performed subcellular fractionation in cells with *SPRED2*

knockdown. We observed a reduction in the phosphorylation of RSK2 at S386 (S380 in RSK1), the phosphorylation site that recruits PDK1, and S227 (S221 in RSK1), the site in the active loop of the NTKD that is phosphorylated by PDK1, at the plasma membrane and nucleus in these cells (**Figs. 2.6D and S2.6C**) (18). Together, these data indicate that SPRED2 regulates the phosphorylation of RSK substrates, possibly by modulating its subcellular localization.

RSK binding promotes SPRED2 complex formation with neurofibromin and negative feedback of MAPK signaling

Using the HR1 cell system, we observed that MAPK activation also promoted interaction between SPRED2 and neurofibromin, in a similar manner as SPRED2-RSK2 (**Fig. 2.5C**). These findings led us to hypothesize that RSK2 promotes SPRED2 complex formation with neurofibromin. To test this, we stably expressed SPRED2 or the RSK2 binding deficient mutant F145A in HEK293T cells, and tested SPRED2 interaction with endogenous neurofibromin (**Fig. 2.7A**). We noted a decrease in neurofibromin binding with the SPRED2 F145A mutant compared to WT. Furthermore, we observed that inserting the RID from SPRED2 into SPRED1 (SPRED1 chimera), which confers RSK binding capacity to SPRED1, also enhanced binding to neurofibromin compared to SPRED1. These differences in binding were observed both in normal serum media and Epidermal Growth Factor (EGF) stimulated conditions, further suggesting that RSK2 promotes SPRED2-neurofibromin complex formation (**Fig. 2.7B and S2.7A**). Since neurofibromin is a negative regulator of the RAS-MAPK pathway, we hypothesized that this deficiency in SPRED2 binding has functional consequences on MAPK signaling. To test this, we performed an EGF time course stimulation and observed that cells expressing SPRED2 F145A had higher RAS activation (as assessed by RAS GTP loading) and elevated ERK1/2 phosphorylation, compared to cells expressing SPRED2 WT (**Fig. 2.7C**). Given the importance of

SPREDs in neurofibromin membrane localization, we hypothesized that this difference in MAPK activation may be due to the inability of SPRED2 F145A to localize neurofibromin to the plasma membrane. However, when performing subcellular fractionation, we observed no statistically significant difference in neurofibromin membrane localization between SPRED2 F145A mutant and SPRED2 expressing cells (**Fig. S2.7B**).

DISCUSSION

In this work, we have conducted a systematic analysis of the SPRED interactome and identified common and unique interactors among the SPRED family that suggest unique functions of these proteins. Here, we focused on the biochemical properties of the interaction between SPRED2 and RSK2 and demonstrate that this interaction is implicated in regulating RSK and the negative feedback of MAPK signaling. While kinase-substrate interactions are typically transient, we report a strong molecular interaction between RSK2 and SPRED2 and characterize SPRED2 as a RSK substrate (26, 27). Recent reports have identified several viral and bacterial proteins that hijack RSK proteins through a conserved DDVF motif (23, 28). A crystal structure of the Kaposi's sarcoma-associated herpesvirus protein (ORF45) bound to RSK2 shows that the DDVFT motif of ORF45 binds and interacts with RSK2 in a similar manner as SPRED2 (**Fig. S2.4C**). However, unlike SPRED2, ORF45 uses additional ~45 residues to interact with RSK2 forming a complex with an affinity of ~1 nM, approximately 8000-fold tighter than the RSK2-SPRED2 interaction that we have described (Fig. S4D). This interaction allows ORF45 to hijack the cell to promote pathogen replication (23). In addition to regulating the ability of RSK to phosphorylate substrates, our findings demonstrate that SPRED2 plays an important role in modulating RSK's subcellular localization. Localization to the membrane is a step of RSK activation and previous work has

shown that the proximity of RSK1 to RAS depends on SPRED2 (29, 30). This is consistent with our findings and supports our model that SPRED2 regulates phosphorylated RSK at the membrane, presumably to facilitate negative feedback of MAPK signaling (**Fig. 2.8, A and B**).

Additionally, we speculate that the SPRED2-RSK complex provides an extra layer of regulation for MAPK signaling. Our finding shows that SPRED2-RSK complex formation is regulated by MAPK activation. Upon MAPK stimulation, active ERK1/2 phosphorylates RSK2 at T369, S365, and T577 (T363, S359, and T573 in RSK1) (17). This activates the RSK-CTKD and results in auto-phosphorylation at S386 (31). PDK1 binds at the S386 (S380 in RSK1) phosphorylation site, and then phosphorylates S227 (S221 in RSK1) on the RSK NTKD, allowing RSK to activate and phosphorylate substrates (31, 32). We suspect that phosphorylation by ERK1/2 relieves autoinhibition of RSK and causes a conformational change to promote SPRED2 binding. Our study highlights the crucial role of the interaction between SPRED2 and RSK in the negative regulation of MAPK signaling. Disruption of this interaction leads to hindered interaction with neurofibromin, which in turn results in elevated MAPK signaling (**Fig. 2.8A**). This finding is consistent with previous reports that RSK2 plays a role in the negative feedback of RAS-MAPK signaling (31, 32). By elucidating the molecular determinants of the SPRED2-RSK interaction, our study provides a mechanism for negative feedback. Moreover, our proposed model suggests a dual layer of regulation to ensure negative feedback of MAPK signaling, wherein SPRED2 binds and localizes phosphorylated RSK at the membrane, leading to alterations in RSK substrate phosphorylation. Although our studies did not reveal any significant quantitative effects on neurofibromin membrane localization between SPRED2 WT and SPRED2 F145A expressing cells, this plausible mechanism requires further investigation using more sensitive methodology in future studies (**Fig. S2.7B**).

Phosphorylation of substrates by RSK2 is important during development; thus, germline loss-of-function variants in *RPS6KA3*, the gene encoding RSK2, cause Coffin-Lowry syndrome, a disorder characterized by growth and developmental delay as well as other skeletal anomalies (33–36). The recent identification of *SPRED2* loss-of-function variants in individuals with Noonan syndrome, which also has phenotypic skeletal features, suggests a genetic link between SPRED2 and RSK2 with implications for proper skeletal development (11, 37).

An additional interaction we identified was between SPRED3 and 14-3-3 proteins. While pathogenic mutations in *SPRED3* have not been reported, both SPRED3 and 14-3-3 proteins are highly expressed in the brain, suggesting an important neuronal function of SPRED3 (6, 38). Further analysis of this interaction may shed light on a function of SPRED3 that cooperates with 14-3-3 proteins in the context of neuronal development.

In all, our screening results show ways in which SPRED proteins evolved to have unique protein binding partners that, in turn, delegates their functions and alters how they can regulate signaling.

Figures

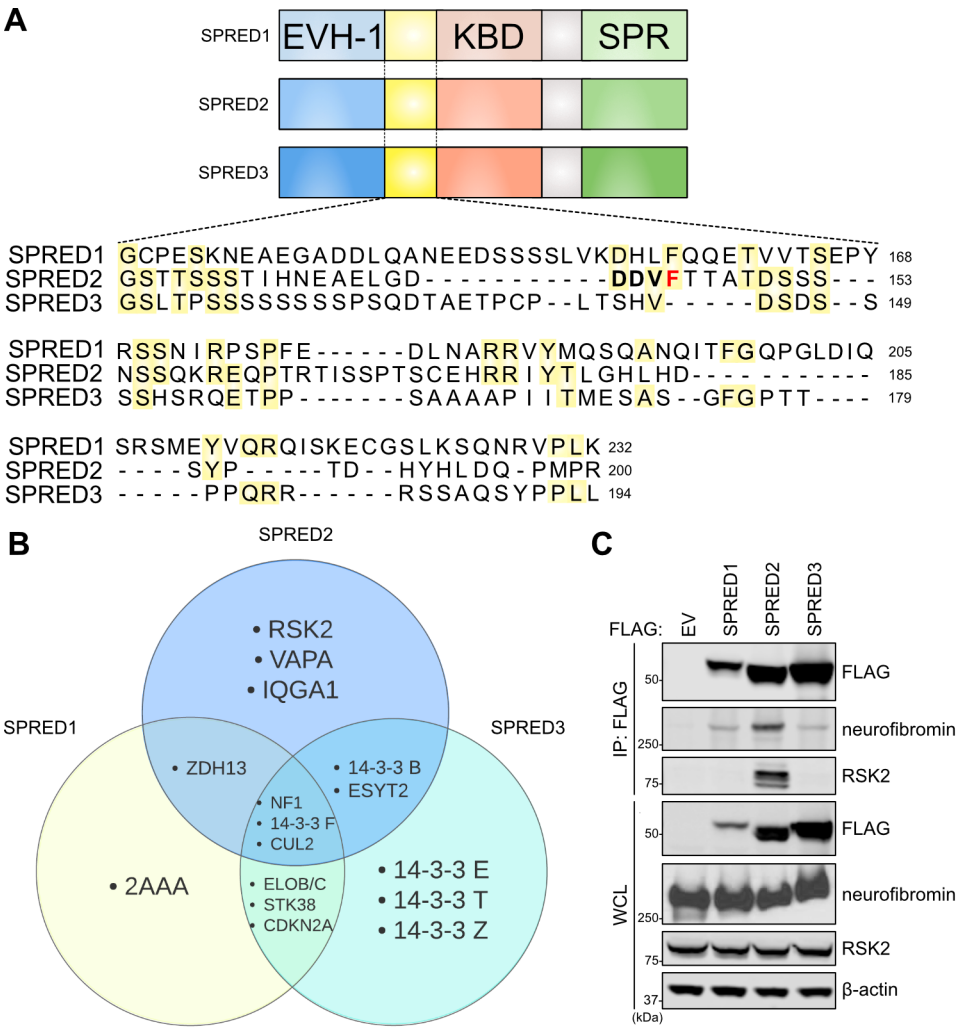

Figure 2.1. A proteomic screen reveals common and unique interactors of SPRED proteins

A, Schematic of SPRED1-3 domain structure and alignment of the uncharacterized unique domains found between EVH-1 and KBD. EVH-1: Ena/Vasp Homology; KBD: KIT binding domain; SPR: sprouty related domain. ***B***, Venn diagram of SPRED protein binding partners identified from affinity purification mass spectrometry screen. 2AAA (Serine/ threonine-protein phosphatase 2A regulatory subunit A alpha isoform); RSK2 (serine/threonine kinase ribosomal protein s6 kinase alpha-2); VAPA (VAMP Associated Protein A; IQGA1 (Ras GTPase-activating-like protein); ELOB/C (Elongin-B/ C); STK38 (Serine/ threonine kinase 38); CDKN2A (Cyclin-dependent kinase inhibitor 2A); NF1 (neurofibromin); ZDH13 (Palmitoyltransferase ZDHHC13); CUL2 (Cullin-2); 14-3-3 protein B (beta), F (eta), T (theta), Z (zeta). ***C***, Immunoblot of indicated proteins from a co-immunoprecipitation of FLAG tagged SPRED proteins expressed in HEK293T cells. Empty vector (EV); WCL (whole cell lysate); IP (immunoprecipitation).

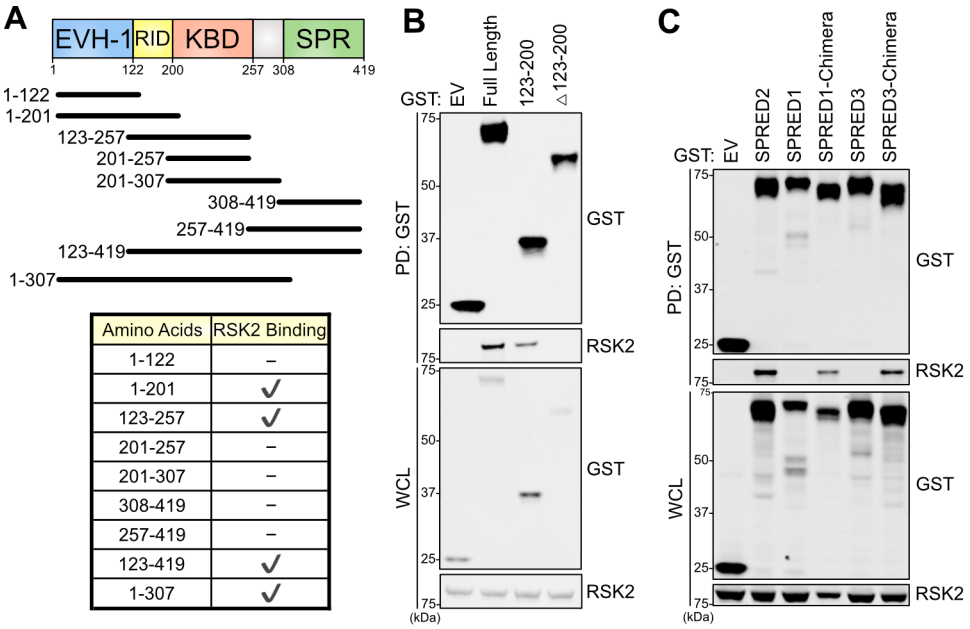

Amino Acids	RSK2 Binding
1-122	–
1-201	✓
123-257	✓
201-257	–
201-307	–
308-419	–
257-419	–
123-419	✓
1-307	✓

Figure 2.2. SPRED2 interacts with RSK2

A, Truncation mutations of SPRED2 expressed in HEK293Ts and immunoblotted to assess for binding to endogenous RSK2. EVH-1 (Ena/Vasp Homology); RID (RSK interacting domain); KBD (KIT binding domain); SPR (sprouty related domain). ***B-C***, Immunoblots of indicated proteins from a pulldown of GST -EV, -SPRED2, -SPRED2 mutants, -SPRED1, or -SPRED3 expressed in HEK293T cells. Empty vector (EV), SPRED1-Chimera/ SPRED3-Chimera (SPRED1/3 construct replaced with corresponding SPRED2-RID amino acids), WCL (whole cell lysate); IP (immunoprecipitation).

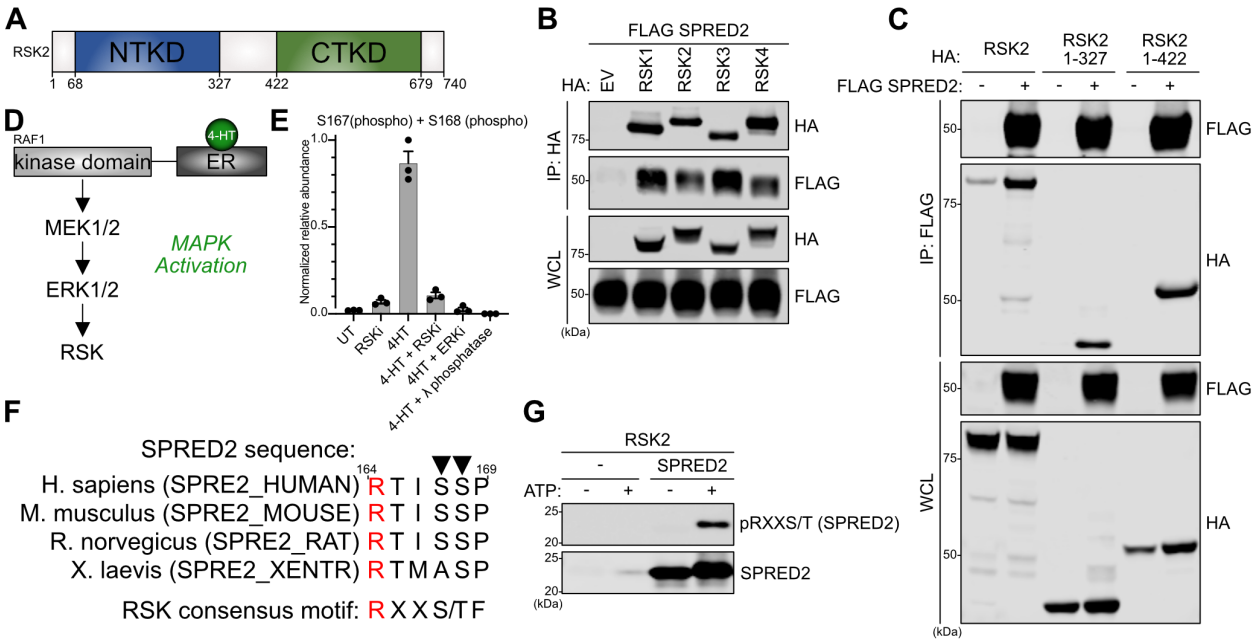

Figure 2.3. SPRED2 interacts with RSK family and is phosphorylatable

A, Schematic of RSK2 domain architecture. NTKD (N-terminal kinase domain); CTKD (C-terminal kinase domain). ***B-C***, Immunoblots of indicated proteins from a co-immunoprecipitation of HA-RSK(1-4) or -RSK mutants expressed in HEK 293T cells. ***D,*** Schematic of HR1 cell system; ER (estrogen receptor). ***E,*** Analysis of phosphorylation events on FLAG-SPRED2-expressing HR1 cells treated with 200 nM 4-HT for 2 h with 4-HT (4-hydroxytamoxifen) and the indicated kinase inhibitors or λ phosphatase (lambda phosphatase). Relative qualification of the peptide abundance in three biological replicates based on extracted MS1 chromatographic peaks of. Bars represent mean normalized relative abundance, and error bars show the corresponding standard deviation. ***F,*** Analysis of AGC Kinase phosphorylation motif RXX(S/T). [R, arginine; X, any amino acid; (S/T) phosphorylatable serine or threonine]. R1 highlights in red, and phosphorylatable S is indicated by the black triangle. Alignment was performed with Uniprot using SPRED2 protein sequences from humans (*Homo sapiens*), mouse (*Mus musculus*), rat (*Rattus norvegicus*), and frog (*Xenopus laevis*). ***G,*** SPRED2 (104-297) recombinant protein was subjected to in vitro kinase assay and immunoblotted for phosphorylation by RSK2 with pRXXS/T antibody. Empty vector (EV); WCL (whole cell lysate); IP (immunoprecipitation).

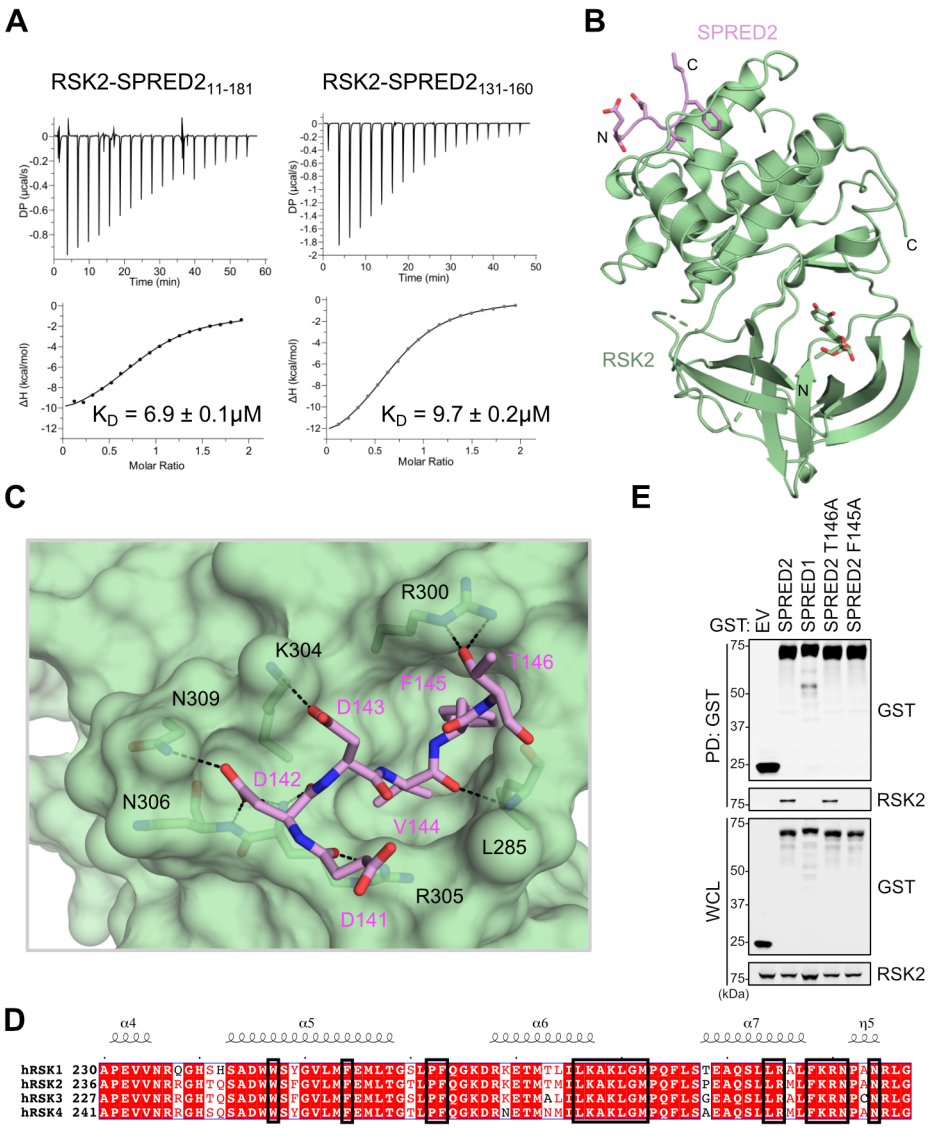

Figure 2. 4 : Structural analysis of the SPRED2-RSK2 interaction

A, Isothermal titration calorimetry of RSK2 (44-367) with SPRED2 (11-181) (left) or SPRED2 (131-160) (right). Dissociation constant (K_D) is shown as a mean ±SD. ***B***, The 1.8 Å crystal structure of RSK2 (46-346) (green) in complex with SPRED2 (131-160) (pink) shown as a cartoon. The pan-RSK ligand (quercitrin) bound to the active site is shown as green sticks. ***C***, SPRED2 peptide (shown as pink sticks) bound to the surface of RSK2 (green). Hydrogen bonds are shown as black dashes. ***D***, Sequence alignment of all four human members of the RSK family. Residues which SPRED2 contact on RSK2 are shown in black boxes. Conserved and non-conserved residues are shown in red and white, respectively. ***E***, Immunoblot of indicated proteins from a pulldown of GST- EV, -SPRED2, or -SPRED2 mutants expressed in HEK293T cells. Empty vector (EV); WCL (whole cell lysate); PD (pull down).

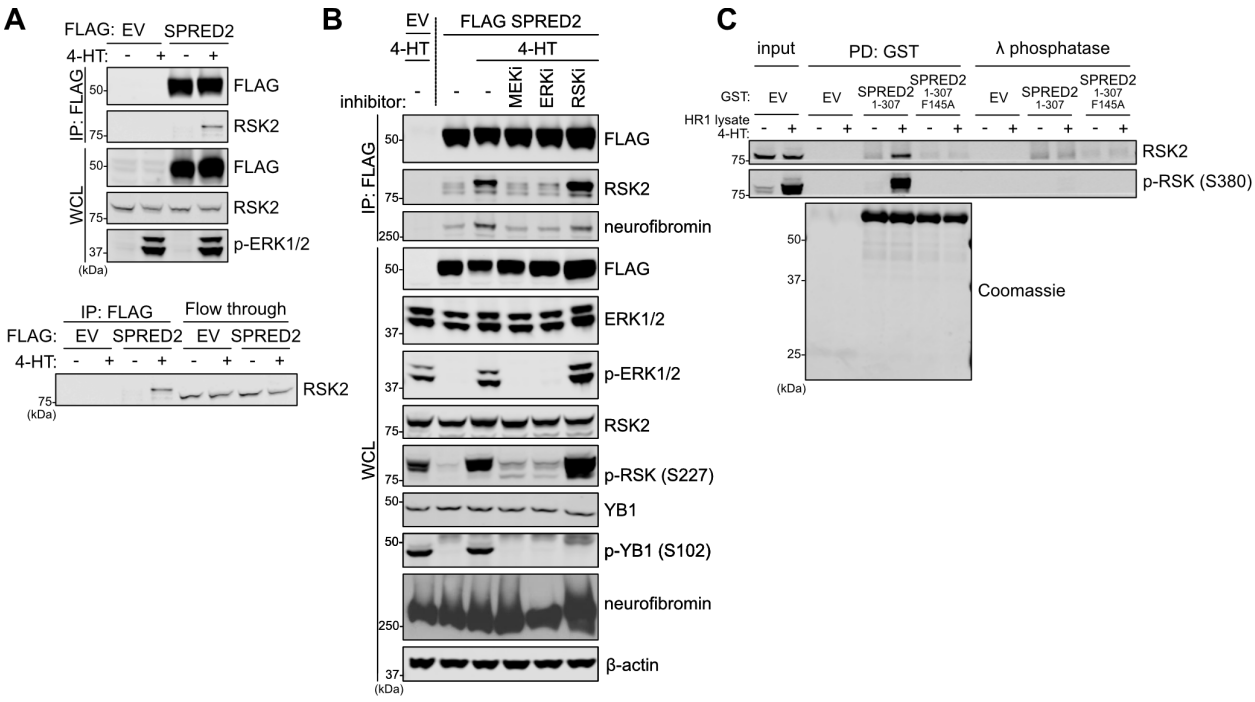

Figure 2.5. SPRED2 /RSK interaction is regulated by MAPK activation

A, Immunoblot of indicated proteins from a co-immunoprecipitation of FLAG-SPRED2-expressing HR1 cells treated with 200 nM 4-HT for 2 h. Co-immunoprecipitate and flow through were immunoblotted for endogenous RSK2. ***B***, FLAG-SPRED2-expressing HR1 cells were treated with 4-HT and the indicated kinase inhibitors. FLAG-immunoprecipitates and non-binding lysates (flow through) were probed for interacting proteins and phosphorylated proteins respectively. ***C***, Immunoblot of indicated proteins from a pulldown of GST -EV, -SPRED2 and -SPRED2 F415A purified from bacteria, were probed for endogenous RSK2 binding following incubation with lysate from HR1 cells. Empty vector (EV); WCL (whole cell lysate); IP (immunoprecipitation); PD (pull down).

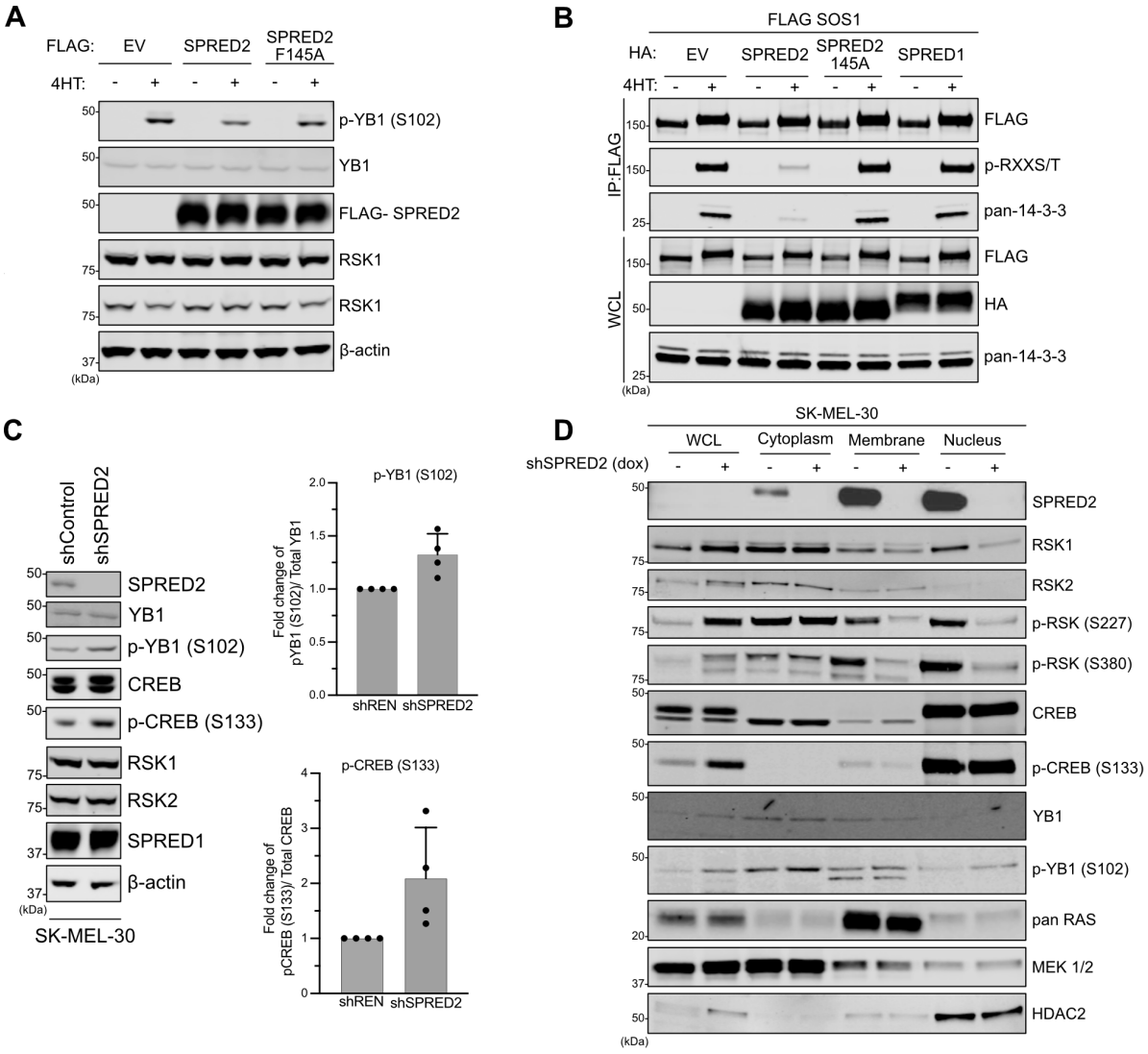

Figure 2.6. SPRED2 regulates phosphorylation of RSK substrates and subcellular localization

A, Immunoblot of indicated proteins from HR1 cells expressing FLAG-tagged EV, SPRED2, or SPRED2 F145A. ***B,*** Immunoblot from a co-immunoprecipitation of HR1 cells co-expressing FLAG-SOS1 and HA-tagged EV, SPRED2, SPRED2 F145A, or SPRED1. ***C,*** Immunoblots showing *SPRED2* stably knocked down in SK-MEL-30 cells. Relative qualification based on densitometry of the pCREB and pYB1 in four biological replicates. Bars represent mean fold change, and error bars show the corresponding standard deviation. Knockdown was induced in cells with doxycycline (1 µg/mL) treatment. ***D,*** Immunoblot of subcellular fractionation from SK-MEL-30 cells with *SPRED2* knocked down. Empty vector (EV); WCL (whole cell lysate); IP (immunoprecipitation).

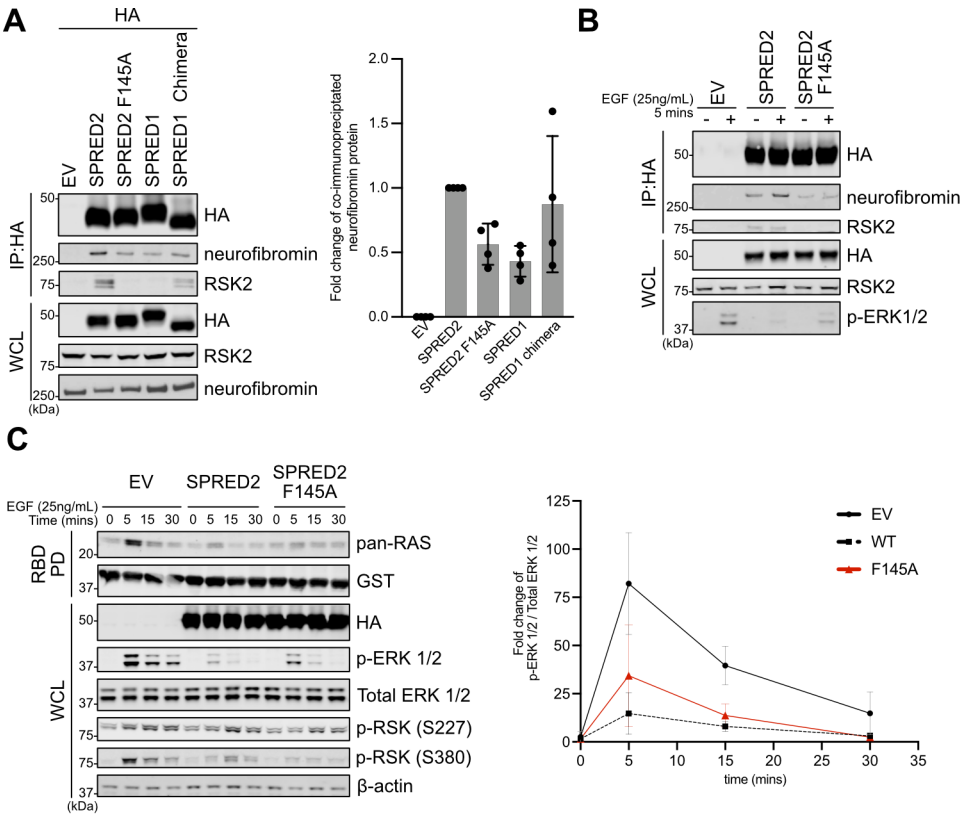

Figure 7. RSK2 negative feedback of MAPK signaling through regulation of SPRED binding to neurofibromin

A-C, Immunoblots of HEK293T cells with stable expression of HA-tagged EV, SPRED2, SPRED2 F145A, SPRED1, or SPRED1 chimera probing against endogenous neurofibromin and RSK2. Relative qualification based on densitometry of neurofibromin in four biological replicates. Bars represent mean fold change, and error bars show the corresponding standard deviation. ***C***, Cells were serum starved for 15-18 h and then stimulated for the indicated time with 25 ng/mL of EGF. Relative qualification from biological replicates based on densitometry of the pERK1/2 from three biological replicates. Bars represent mean fold change, and error bars show the corresponding standard deviation. Lysate was incubated on RBD-GST beads and immunoblotted against endogenous pan-RAS. Empty vector (EV); WCL (whole cell lysate); IP (immunoprecipitation); RBD PD (RAS binding domain pull down).

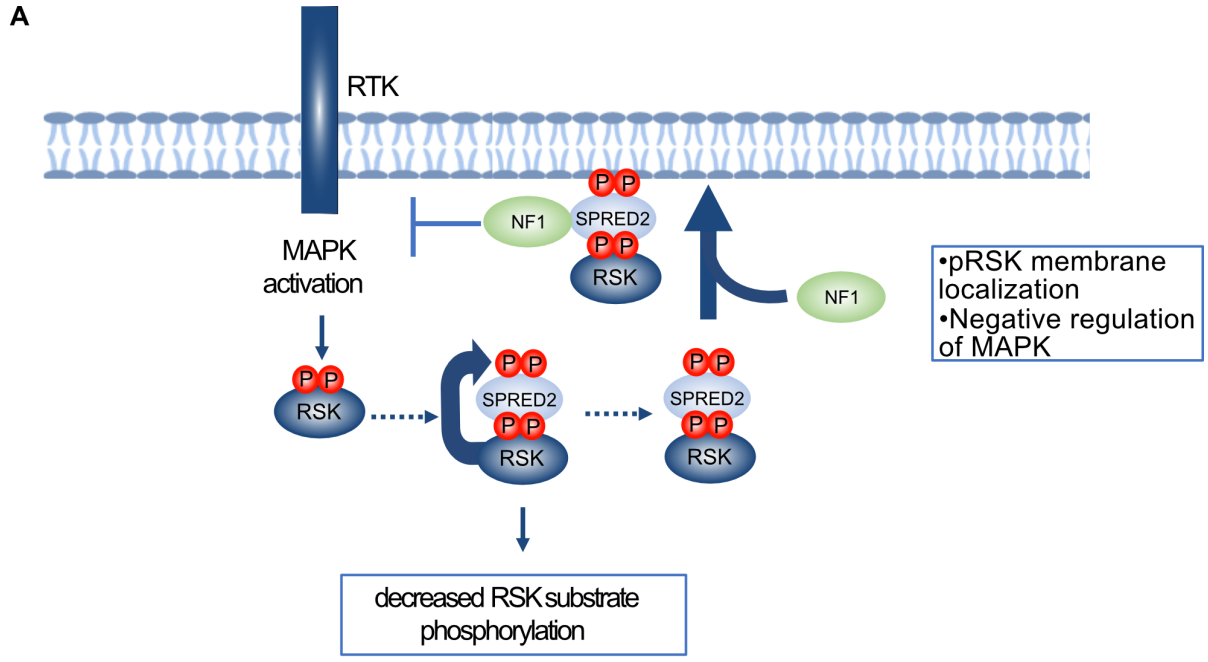

Figure 8. A RSK -SPRED2 complex regulates phosphorylation of RSK substrates and MAPK signaling

A, Formation of the SPRED2-RSK complex is regulated by MAPK activation. SPRED2 binding perturbs phosphorylation of other RSK substrates and leads to SPRED2 phosphorylation. SPRED2 binding promotes pRSK membrane translocation. RSK binding enhances NF1 interaction with SPRED2, leading to negative feedback on MAPK signaling.

Table 2.1 Crystallographic data collection and refinement statistics

	$RSK2_{46-346}$ -$SPRED2_{131-160}$
Data collection	
Space group	I 1 2 1
Cell dimensions	
a, *b*, *c* (Å)	83.44, 41.10, 99.26
α, β, γ (°)	90.0, 113.89, 90.0
Resolution (Å)	49.39-1.80 (1.84-1.80) *
R_{merge}	0.059(0.771)
R_{pim}	0.057(0.752)
$I / \sigma I$	8.8(1.4)
Completeness (%)	97.7(98.8)
Redundancy	3.3(3.3)
CC(1/2)	0.99(0.57)
Refinement	
Resolution (Å)	49.39-1.80
No. reflections	93088
R_{work} / R_{free}	18.3/22.5
No. atoms	
Protein	2343
Ligand/ion	32
Water	139
B-factors	
RSK2	38.9
SPRED2	62.7
Ligand/ion	31.2
Water	40.3
R.m.s. deviations	
Bond lengths (Å)	0.007
Bond angles (°)	0.903

Supporting information

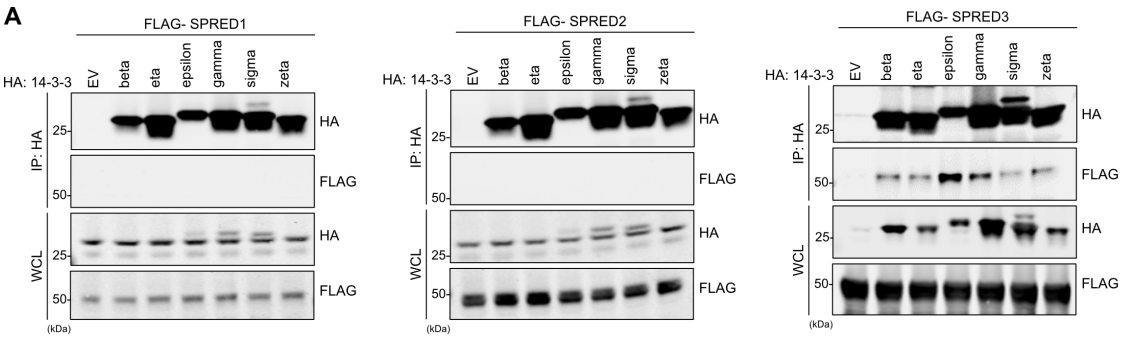

SFigure 2.1. A proteomic screen of SPRED proteins

A, Co-immunoprecipitation of HA-14-3-3 family with FLAG SPRED1-3, expressed in HEK293T cells. Empty vector (EV); WCL (whole cell lysate); IP (immunoprecipitation).

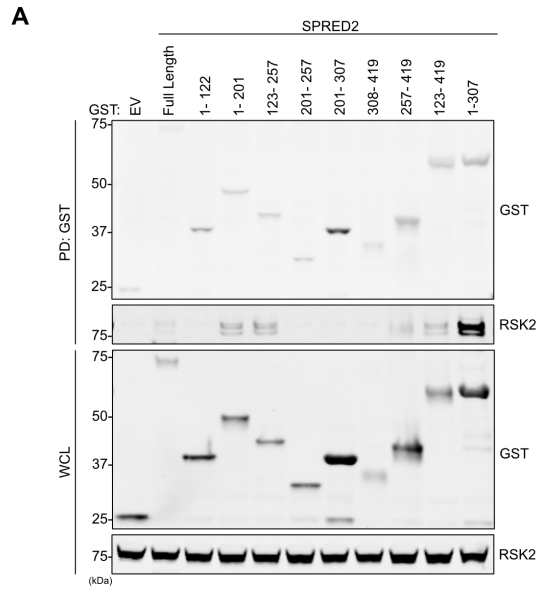

SFigure 2.2. Analysis of SPRED2 interaction with RSK2

A*,* GST tagged truncations of SPRED2 expressed in HEK293Ts and immunoblotted to assess for binding to endogenous RSK2. Empty vector (EV); WCL (whole cell lysate); IP (immunoprecipitation).

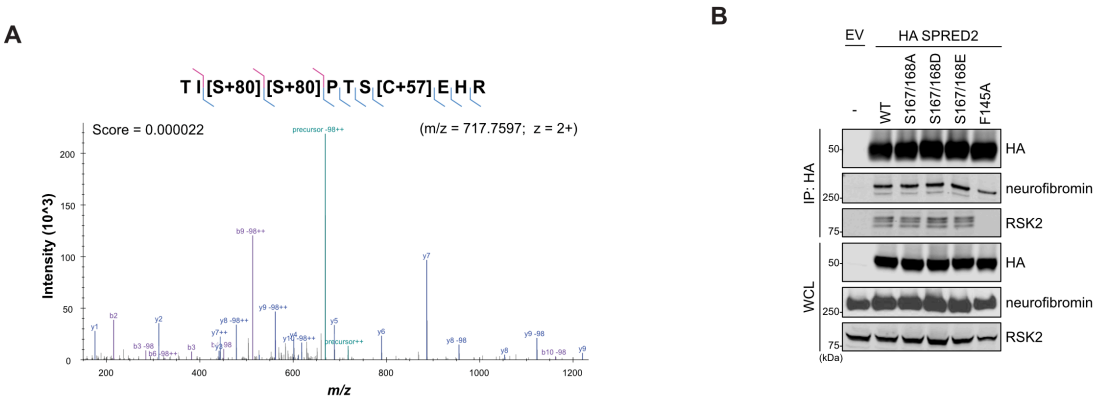

SFigure 2.3. SPRED2 phosphorylation at S167+S168.

A, Annotated MS2 spectrum of the double phosphorylated SPRED2 peptide. The expectation score for the spectrum is shown. ***B,*** Immunoblots of HEK293T cells with stable expression of HA-tagged EV, SPRED2, SPRED2 S167/S168A, SPRED2 S167/S168D, SPRED2 S167/S168E, or SPRED2 F145A probing against endogenous neurofibromin and RSK2. Empty vector (EV); WCL (whole cell lysate); IP (immunoprecipitation).

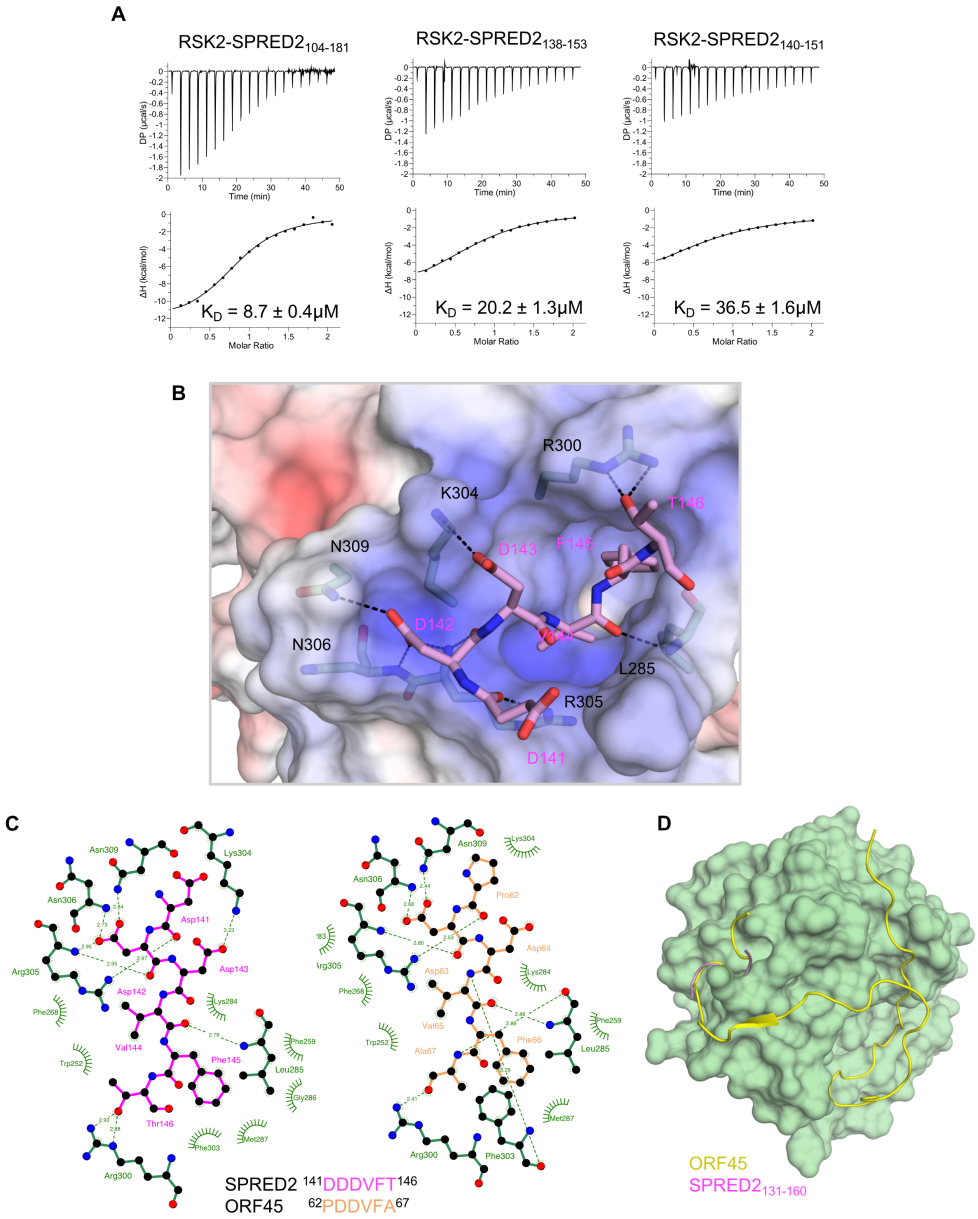

SFigure 2.4. Structural analysis of the SPRED2-RSK2 interaction.

A, Isothermal titration calorimetry of RSK244-367 with SPRED2104-181, SPRED2138-153 and SPRED2140-151. ***B,*** SPRED2 peptide (shown as pink sticks) bound to the electrostatic surface of RSK2 (blue – positively charged, white – neutral, red – negatively charged). Hydrogen bonds are shown as black dashes. ***C,*** Ligplot diagram showing the RSK2-SPRED2 (left, green and pink, respectively) and the RSK2-ORF45 (right, green and orange, respectively) interactions. ***D,*** Superposition of the RSK2-ORF45 (yellow) and RSK2-SPRED2 (pink) structures.

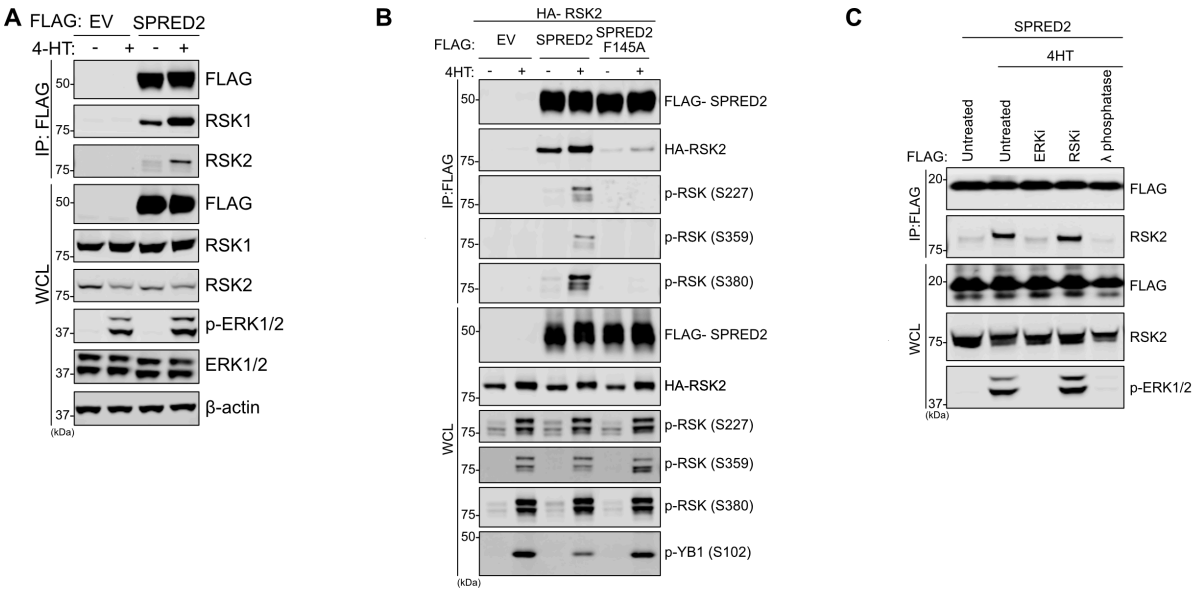

SFigure 2.5. SPRED2 /RSK interaction is regulated by MAPK activation

A, Immunoblot of indicated proteins from a co-immunoprecipitation of FLAG-SPRED2-expressing HR1 cells treated with 200 nM 4-HT for 2 h. Co-immunoprecipitate and flow through were immunoblotted for endogenous RSK1 and RSK2. ***B,*** HA RSK2 and FLAG SPRED2- WT or SPRED2 F145A were expressed in HR1 cells. Cells were treated with 4-HT (200nM) for 2 hrs, immunoprecipitated with FLAG beads and blotted against HA RSK and pRSK (S227, S359, or S380). ***C,*** FLAG SPRED2- WT or SPRED2 F145A were expressed in HR1 cells. Cells were treated with 200 mM 4-HT and ERKi (SCH772984,1 μM), RSKi (LJH685, 10 μM) or λ phosphatase and immunoblotted for endogenous RSK2 binding. Empty vector (EV); WCL (whole cell lysate); IP (immunoprecipitation).

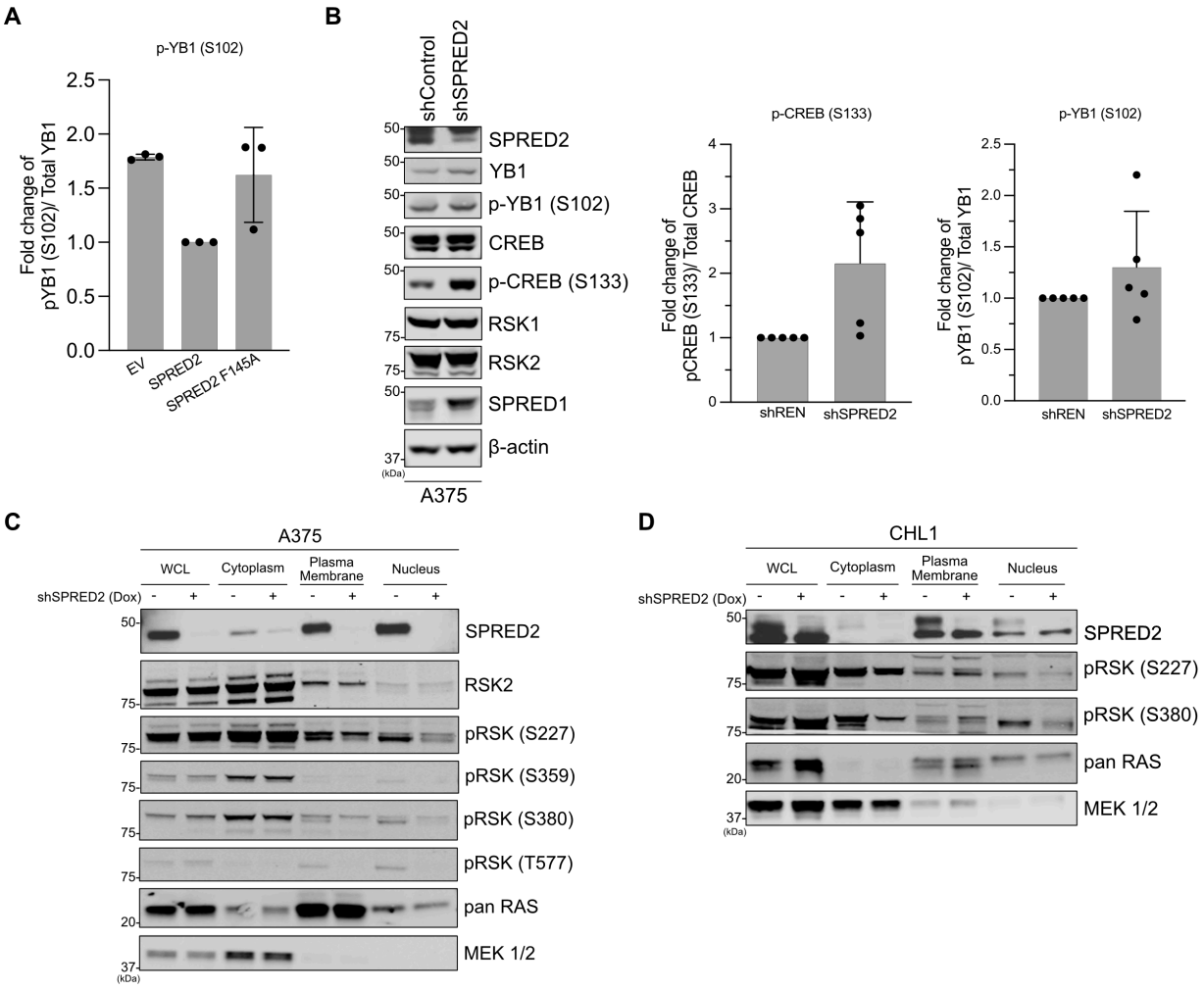

SFigure 2.6. Fractionation in A375 and CHL1 cells

A, Relative qualification based on densitometry of pYB1 in three biological replicates from immunoblots in Fig 6A. Bars represent mean fold change, and error bars show the corresponding standard deviation. ***B***, Immunoblots showing *SPRED2* stably knocked down in A375 cells. Relative qualification based on densitometry of pCREB and pYB1 in five biological replicates. Bars represent mean fold change, and error bars show the corresponding standard deviation. Knockdown was induced in cells with doxycycline (1 µg/mL) treatment. ***C-D***, Immunoblots of subcellular fractionation from A375 and CHL1 cells with knock down of SPRED2.

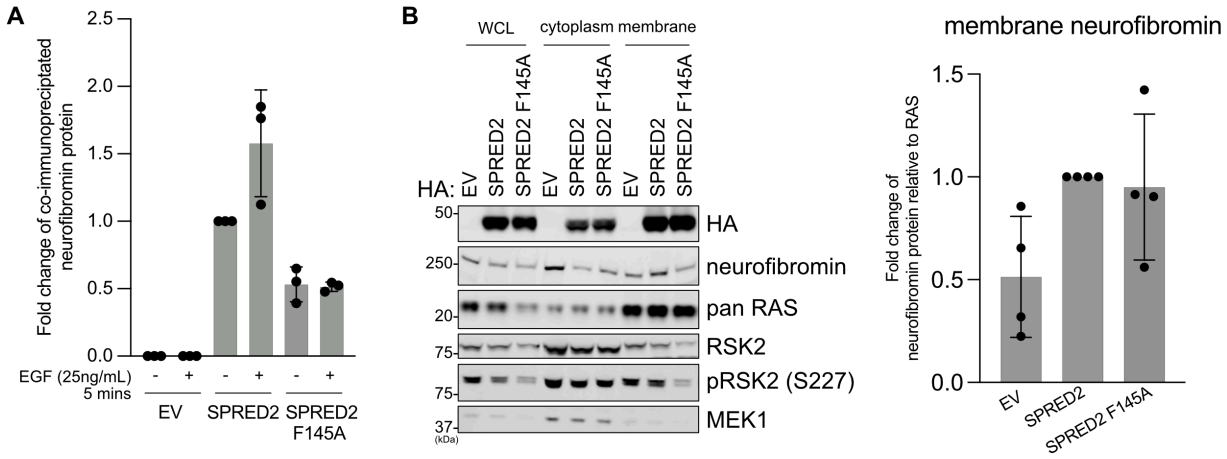

SFigure 2.7. Quantification of neurofibromin binding and membrane localization

A, Relative qualification based on densitometry of neurofibromin in three biological replicates from immunoblots in Fig 7A. Bars represent mean fold change, and error bars show the corresponding standard deviation. ***B,*** Immunoblot of subcellular fractionation in HEK293T cells with stable expression of HA-EV, SPRED2, or SPRED2 F145A. Qualification based on densitometry of neurofibromin relative to RAS in four biological replicates. Bars represent mean fold change, and error bars show the corresponding standard deviation. Empty vector (EV); WCL (whole cell lysate)

EXPERIMENTAL PROCEDURES

Cells and culture conditions

HEK293T, A375, CHL-1, and H441 cells were obtained from the American Type Culture Collection (ATCC), and SK-MEL-30 cells were from DSMZ (Leibniz Institute DSMZ-German Collection of Microorganisms and Cell Cultures, Braunschweig, Germany). HEK293 ΔRaf-1:ER* (HR1) cells were kindly provided by Simon Cook (Babraham Institute, Cambridge, UK). HEK293T, A375, CHL1, and HR1 cells were cultured in Dulbecco's modified Eagle's medium (DMEM) supplemented with 10% Fetal Bovine Serum (FBS) and Penicillin-Streptomycin. HR1 cells were supplemented with 1 mg/mL G418. SK-MEL-30 were cultured in Roswell Park Memorial Institute (RPMI) 1640 media supplemented with 10% Fetal Bovine Serum (FBS) and Penicillin-Streptomycin. Cell lines were regularly tested with MycoAlert PLUS Mycoplasma Detection Kit (Lonza).

Reagents, antibodies, and immunoblotting

Antibodies against Neurofibromin 1 (#14623; 1:1000), RSK2 (5528; 1:1000), HA-Tag (#3724; 1:1000), Phospho-RSK2 (Ser227) (#3556; 1:1000), Phospho-p90RSK (Ser380) (#11989; 1:1000), Phospho-Akt Substrate (RXXS*/T*) (#9614; 1:1000), Phospho-p44/42 MAPK (Erk1/2) (Thr202/Tyr204)(#4370; 1:1000), p44/42 MAPK (Erk1/2) (#4696; 1:1000), CREB (#4820; 1:1000), Phospho-CREB (Ser133) (#9198; 1:1000), Phospho-YB1 (Ser102) (#2900; 1:1000), MEK1/2 (# 8727; 1:1000) were all purchased from Cell Signaling Technology. Antibodies against GST Antibody pan (#sc-138; 1:1000) and 14-3-3 Antibody (#sc-629; 1:1000) were purchased from Santa Cruz Biotechnology. ANTI-FLAG (# F7425) and β-Actin (A5441) were purchased from Sigma-Aldrich and THE™ DYKDDDDK (#A00187;) was purchased from GenScript, and pan

RAS (#108601; 1:1000) was purchased from Abcam. A customized rabbit polyclonal antibody against Spred2_122-212aa was generated with GenScript. Lysates were prepared with RIPA Buffer (150mM NaCl, 1% NP-40, 0.5% Deoxycholate, 0.1% SDS, 50 mM Tris-HCl 7.5) and normalized to load 20-30 µg of protein. Immunoblots were performed with Bis-Tris NuPAGE gels (Life Technologies) and transferred on nitrocellulose membranes. Membranes were blocked at room temperature for 1 h in 5% skimmed milk in TBS-T buffer. Primary antibodies were diluted in 3% BSA and incubated at 4°C overnight. Immunoblots were developed by washing with TBS-T three times and then incubating with secondary antibodies; DyLight680 (611-144-002; 1:10,000) or DyLight800 (610-145-002; 1:10,000) (Rockland), and scanning with LI-COR Odyssey. To detect SPRED2, HRP conjugated secondary antibodies were used and developed using Immobilon Forte Western HRP Substrate (# WBLUF05000) and HyBlot CL® Autoradiography Film (#XC6A2). Fractionation was performed used Subcellular Protein Fractionation Kit (# 7884) from Thermo Fisher Scientific following manufacturers protocol.

Plasmids, cloning and transfection

SPRED1-3, RSK1-4, and SOS1 entry clones were obtained from the RAS Pathway 2.0 Clone Collection (Addgene #1000000070). SPRED2 plasmids used for mammalian expression were generated by mutagenesis in pDONR255-SPRED2 template: (1-122, 1-201, 123-257, 201- 257, 201-307, 308-419, 257-419, 123-419, 1-307, ∆123-200, 123-200, SPRED2 F145A, SPRED2 1-307 F145A). All 14-3-3 plasmids were obtained from Addgene. SPRED2 ∆KBD, SPRED1 chimera, and SPRED3 chimera were generated as a gene fragment with GenScript. RSK2 plasmids used for mammalian expression were generated by mutagenesis in pDONR255-RSK2 template: (RSK2 1-327, 1-422). All mutagenesis primer sequences are available upon request. All entry clones were generated using BP reactions into DONR255 vectors. All expression vectors were

generated with LR Gateway cloning containing into pDEST302 or pDEST663, EF1α promoter, and either N-terminal 3xFLAG or N-terminal HA tag. All plasmid transfections were performed with jetOPTIMUS® DNA Transfection Reagent (# 101000006) following manufacturers protocol. Genes for protein expression were generated from DNA constructs initially synthesized as Gateway Entry clones (ATUM, Newark, CA). Constructs consisted of *E. coli* gene optimized fragments containing an upstream tobacco etch virus (TEV) protease site (ENLYFQ/G) followed by fragments of the coding sequence of human SPRED2 or human RSK2 (*RPS6KA3*) as defined below. Entry clones were transferred to *E. coli* destination vectors containing aminoterminal His6 (pDest-527, Addgene #11518) or His6-MBP (pDest-566, Addgene #11517) fusions by Gateway LR recombination (Thermo Scientific, Waltham, MA). The shorter RSK2 clone (R765-X33-527) contained an additional non-native tripeptide sequence (Met-Ala-Gly) at the N-terminus of the final construct to improve protein production and crystallization. Constructs generated were: His6-MBP-tev-Hs.SPRED2(11-181); His6-MBP-tev-Hs.SPRED2(104-181); His6-tev-Hs.RSK2(44-367; His6-tev-GMAG-Hs.RSK2(46-346).

Lentiviral transduction

Constructs for stable lentiviral expression were generated as described above with pDEST663 vector. HEK293T cells were co-transfected with the construct of interest, pδ8.91, and pMD2.G in in a 3:2:1 ratio, respectively. 48 h post-transfection, supernatant was collected, passaged through 0.45 μm filter, and transduced into cells with polybrene. Cells were cultured with the appropriate selection media to select for expressing cells.

To generate knock-down cell lines, miR-E constructs were designed to target *SPRED2* as previously reported (39). Lentiviral particles were generated using these miR-E constructs

(LT3GEPIR), as described above, and transduced into cells. Cells were kept in culture with puromycin (0.5 μg/mL) and doxycycline (1 μg/mL) was used to induce knockdown.

Bacterial protein expression and purification

Proteins were expressed as described for the Dynamite expression protocol (40). Proteins were purified essentially as previously outlined for KRAS (1-169) with some exceptions. Specifically, the Hs.SPRED2(104-181), Hs.RSK2(44-367), and GMAG-Hs.RSK2(46-346) purifications included 300 mM NaCl and 10% glycerol (w/v) in all buffers, $MgCl_2$ was omitted, and the final buffer was 20 mM HEPES, pH 7.4, 300 mM NaCl, 1 mM TCEP, and 10% glycerol (w/v) (41). Final buffer for Hs.SPRED2 (11-181) was 20 mM HEPES, pH 7.4, 150 mM NaCl, and 1 mM TCEP. Recombinant GST-tagged proteins -EV, -SPRED2 1-307, and -SPRED2 1-307 F145A were generated by gateway cloning into pGEX-6. Plasmids were then transformed into BL21 (DE3) cells. Cultures were inoculated with starter cultures and grown at 37°C for 3-4 h. Following, expression was induced with 0.2mM IPTG for 14-16 h at 18°C. Cells were lysed in 50mM Tris HCl (pH 8.0), 300mM NaCl, 5% glycerol, 1mM DTT by sonication. Lysate was put over Glutathione Sepharose 4B beads (Cytiva Life Sciences), washed, and stored in 50% glycerol at -20°C.

Immunoprecipitation and GST pulldown assays

Cells were lysed in buffer containing 150mM NaCl, 1% IGEPAL CA-630, 10% Glycerol, 50 mM Tris-HCl 7.5 with Phosphatase Inhibitor Cocktail 1(P2850; 1:100), Phosphatase Inhibitor Cocktail 2 (P5726; 1:100), and Protease Inhibitor Cocktail (mammalian cell extracts) (P8340; 1:100) from Sigma-Aldrich. Lysates were rotated for 1 h at 4°C with Glutathione Sepharose 4B beads (Cytiva Life Sciences), ANTI-FLAG® M2 Affinity Gel (Sigma), or Pierce™ Anti-HA Agarose (ThermoFisher Scientific). Beads were washed three times with lysis buffer and resuspended with

LDS sample buffer. For immunoprecipitation from HR1 cells, cells were treated with 200 nM 4-HT for 2 h and with 100 nM trametinib (MEKi), 1 μM SCH772984 (ERKi), or 10 μM LJH685 (RSKi) where indicated.

To measure RAS.GTP levels, cells were serum starved for 15-18 h and stimulated with 25 ng/mL of Epidermal Growth Factor (EGF). Lysates rotated for 1h at 4°C with RBD-GST beads.

Kinase Assays

Recombinant RSK2 was purchased from SignalChem (R17-10G) and SPRED2 was made as described in bacterial protein expression and purification section. Reactions contained 100 ng of RSK2, 1 μg of SPRED2, and 1 mM of ATP (Sigma- Aldrich; #A7699). Reaction were brought up to 25 μL with Kinase Assay Buffer (5 mM MOPS, pH7.2, 2.5 mM β-glycerol-phosphate, 10 mM MgCl2, 1 mM EGTA, 0.4 mM EDTA, 50 ng/ml BSA) and were incubated at 30°C and were stopped after 15 min with LDS sample buffer.

Mass Spectrometry

To evaluate bindings partners, 5 μg of 3x-FLAG-SPRED1-3 was transiently transfected into 10^6 HEK293T cells. Cells were lysed as described above and incubated with magnetic flag beads.

To evaluate phosphorylation events on SPRED2, 5 μg of 3x-FLAG-SPRED2 was transiently transfected into 5 x 10^6 HR1 cells. Cells were treated with 4-HT to activated MAPK and co-treated with 1 μM SCH772984 (ERKi) or 10 μM LJH685 (RSKi) for two hours.

Cells were lysed as described above. Conditions with lambda phosphatase were treated post-lysis, following manufacturers guidelines (New England BioLabs; P0753S). The lysates were then incubated with magnetic flag beads.

The beads were washed with ice-cold 20 mM Tris-HCl (pH 8.0), 2 mM CaCl2 buffer and frozen prior to trypsin digest. On-bead trypsin digests were performed as previously described (42).

Digested peptides were desalted with ZipTip u-C18 pipette tips (Millipore), vacuum dried, and reconstituted in 15 μL of 0.1% formic acid. 2.5 uL of each sample were injected on Acquity UPLC M-Class system (Waters) and analyzed by LC-MS/MS on Orbitrap Fusion Lumos Tribrid Mass Spectrometer (Thermo Fisher Scientific) equipped with 15 cm silica-C18 EasySpray column (Thermo Fisher Scientific). The column was operated at 45°C, and reversed-phase chromatography was performed using conventional two-buffer system (Buffer A - 0.1% formic acid in water; Buffer B - 0.1% formic acid in acetonitrile) at 400 nL/min flow rate, as follows: Load at 2% B for 20 min; 2-60% B gradient over 60 min; brief wash at 80% B; equilibration at 2% B. The mass spectrometer was operated in DDA (Full-MS/ddMS2) mode with one survey scan (375-1500 m/z, R=120,000, AGC target of 4e5) followed by HCD MS2 scans up to 3 sec limit (AGC target of 5e4, max IT 100 ms, R=30,000, isolation window 1.6 m/z, NCE 30%, stepped collision 5%, and 30 s dynamic exclusion).

Acquired MS data were analyzed as previously described (43). Briefly, spectra were searched using Protein Prospector (version 6.2.4) against human SwissProt database downloaded on 01/18/2021 and corresponding decoy database of randomly shuffled peptide sequences (44–46). Default “ESI-Q-high-res” parameters with trypsin as the protease were used. Up to two missed cleavages were allowed. Carbamidomethyl-C was a constant modification, with default variable modifications plus phosphorylation at STY. Up to 3 modifications per peptide were considered. Mass tolerance was 5 ppm for precursor ions and 15 ppm for fragment ions. False discovery rate was set for <1% for peptides, and at least 3 unique peptides per protein were required. Protein Prospector search results were exported as BiblioSpec spectral library for downstream analysis in Skyline (v21) to quantify peptide and protein abundances (47). Statistical analysis of peptide and

protein abundances in different biological conditions were carried out using MSstats package integrated in Skyline (48).

Peptides

SPRED2 (140-151) (GDDDVFTTATDS), SPRED2 (138-153) (ELGDDDVFTTATDSSS) and SPRED2 (131-160) (STIHNEAELGDDDVFTTATDSSSNSSQKRE) peptides were synthesized by Genscript with the N-terminal residues acetylated.

Isothermal titration calorimetry measurements

Proteins were extensively dialyzed against 50 mM HEPES, 500 mM NaCl, 3 mM β-mercaptoethanol, 5 mM ETDA, pH 8.0. Duplicate ITC measurements were performed on a MicroCal PEAQ-ITC instrument (Malvern Panalytical). An ITC experiment typically consisted of 40-70 μM of RSK2 (44-367) in the cell with 400-700 μM of either purified SPRED2 (11-181) and SPRED2 (104-181), or SPRED2 (131-160), SPRED2 (138-153) or SPRED2 (140-151) peptides in the syringe. All measurements were carried out at 25°C, with a stirring speed of 750 rpm and 19 injections of 2.2 μl injected at 210s intervals. Data analysis was performed using a "one set of sites" model using the MicroCal PEAQ-ITC analysis software (v1.41, Malvern Panalytical).

Crystallization and data collection

RSK2 (46-346) (1.1 ml of 138 μM) was mixed with a 1.1-fold excess of quercitrin (20 mM stock dissolved in ethylene glycol, Selleck Chemicals S3824) and incubated on ice for 15 mins. Protein-ligand complex was dialysis against 50 mM Tris, 600 mM NaCl, 5 mM EDTA, 5 mM β-mercaptoethanol, pH 8.0 for 16 h at 4 °C. No precipitation had occurred, and the volume had increased to 1.35 ml. Quercitrin interferes with UV absorbance, so the concentration was estimated based on the volume change (final concentration ~110 μM). The SPRED2 (131-160) peptide was added at an equimolar ratio from a stock of 1.24 mM stock dissolved in dialysis buffer. The RSK2-

SPRED2 complex was incubated for 1 h on ice before crystallization screening was carried out at 20°C using the sitting-drop vapor diffusion method by mixing the complex with an equal volume of reservoir solution (200 nL:200 nL). A single crystal grew over the course of 5 days in condition B12 of the PEGR$_x$ screen (30% w/v PEG 2K MME, 0.1 M Tris, pH 8.0, Hampton Research). The crystal was cryoprotected with 15% v/v glycerol. Using a single crystal, a 1.8 Å dataset was collected on beamline 24-ID-C at the Advance Photon Source (Argonne).

Structure determination and analysis

The dataset was indexed and integrated with XDS before scaling, truncating, and converting to structure factors with Aimless from the CCP4 suite (49, 50). The Matthews coefficient suggested a single copy of RSK2 (46-346) in the asymmetric unit. Molecular replacement was carried out with MOLREP using RSK2 (PDB 4GUE) as a search model (50). Refinement was initially carried out by Refmac5 and manual building in COOT (51, 52). After a few rounds of refinement, an inspection of the difference (*Fo-Fc*) map showed positive density for the six residues in the 30-mer SPRED2 peptide, suggesting the remaining residues are disordered inside the crystal. Final refinement was carried out in Phenix.Refine with occupancy refinement for the SPRED2 peptide (final occupancy for the SPRED2 peptide was 0.89 (53). Figures were generated with PyMOL (54). All crystallographic and structural analysis software was supported and provided by the SBGrid Consortium (54). Crystallographic data collection and refinement statistics are shown in Table 1.

Data Availability

The atomic coordinates and structure factors of the RSK2-SPRED2 complex have been deposited in the Protein Data Bank and are available under the accession number 8EQ5. The authors confirm

that the data supporting the findings of this study are available within the article and its supporting information.

Supporting information

This article contains supporting information.

Funding and additional information

This work was supported by the NCI 1R35CA197709-01and DOD US Army Med. Res. Acq. Activity W81XWH2010129 to F.M.

P.C.'s work is supported by NCI (K99CA245122) and DOD CDMRP NFRP (W81XWH-20-1-0391).

J.L. and M.C-D are supported by UCSF's IMSD program, funded by the National Institute of General Medical Sciences (5R25GM056847). J.L. is also a UCSF discovery fellow. D.S. and D.A-B. are supported by the NCI (HHSN261200800001E)

Acknowledgments

The authors wish to acknowledge Dominic Esposito, Peter Frank, Simon Messing, Matt Drew, Gulcin Gulten, Ashley Mitchell, Nitya Ramakrishnan, Matt Smith, Kelly Snead, Troy Taylor, and Vanessa Wall from the Protein Expression Laboratory at the Frederick National Laboratory for cloning, protein expression, and protein purification support. We thank the UCSF Mass Spectrometry Facility and A. L. Burlingame for providing MS instrumentation support for this We also thank members of the McCormick lab for their support and input.

Conflict of interests

PC is a founder and advisory board of Venthera, Inc. The other authors declare no competing interests. F.M. is a consultant for the following companies: Amgen; Daiichi Ltd., Frontier Medicines, Exuma Biotech, Ideaya Biosciences, Kura Oncology, Leidos Biomedical Research,

Inc., PellePharm, Pfizer Inc., PMV Pharma and Quanta Therapeutics. F.M. is a consultant and co-founder for the following companies (with ownership interest including stock options): BridgeBio; DNAtrix Inc.; Olema Pharmaceuticals, Inc.; and Quartz. F.M. is the scientific director of the National Cancer Institute (NCI) RAS Initiative at the Frederick National Laboratory for Cancer Research/Leidos Biomedical Research, Inc. F.M. has been recipient of research grants from Daiichi Sankyo, Gilead Sciences and has a current grant from Boehringer-Ingelheim.

References:

1. Roovers, K., and Assoian, R. K. (2000) Integrating the MAP kinase signal into the G1 phase cell cycle machinery. *Bioessays*. 22, 818–826

2. Neben, C. L., Lo, M., Jura, N., and Klein, O. D. (2017) Feedback regulation of RTK signaling in development. *Dev Biol*. 447, 71–89

3. Simanshu, D. K., Nissley, D. V., and McCormick, F. (2017) RAS Proteins and Their Regulators in Human Disease. *Cell*. 170, 17–33

4. Castel, P., Rauen, K. A., and McCormick, F. (2020) The duality of human oncoproteins: drivers of cancer and congenital disorders. *Nat Rev Cancer*. 20, 383–397

5. Wakioka, T., Sasaki, A., Kato, R., Shouda, T., Matsumoto, A., Miyoshi, K., Tsuneoka, M., Komiya, S., Baron, R., and Yoshimura, A. (2001) Spred is a Sprouty-related suppressor of Ras signalling. *Nature*. 412, 647–651

6. Kato, R., Nonami, A., Taketomi, T., Wakioka, T., Kuroiwa, A., Matsuda, Y., and Yoshimura, A. (2003) Molecular cloning of mammalian Spred-3 which suppresses tyrosine kinase-mediated Erk activation. *Biochem Bioph Res Co*. 302, 767–772

7. Stowe, I. B., Mercado, E. L., Stowe, T. R., Bell, E. L., Oses-Prieto, J. A., Hernández, H., Burlingame, A. L., and McCormick, F. (2012) A shared molecular mechanism underlies the human rasopathies Legius syndrome and Neurofibromatosis-1. *Gene Dev*. 26, 1421–1426

8. Yan, W., Markegard, E., Dharmaiah, S., Urisman, A., Drew, M., Esposito, D., Scheffzek, K., Nissley, D. V., McCormick, F., and Simanshu, D. K. (2020) Structural Insights into the

SPRED1-Neurofibromin-KRAS Complex and Disruption of SPRED1-Neurofibromin Interaction by Oncogenic EGFR. *Cell Reports*. 32, 107909–107909

9. Dunzendorfer-Matt, T., Mercado, E. L., Maly, K., McCormick, F., and Scheffzek, K. (2016) The neurofibromin recruitment factor Spred1 binds to the GAP related domain without affecting Ras inactivation. *Proc National Acad Sci*. 113, 7497–7502

10. Brems, H., Chmara, M., Sahbatou, M., Denayer, E., Taniguchi, K., Kato, R., Somers, R., Messiaen, L., Schepper, S. D., Fryns, J.-P., Cools, J., Marynen, P., Thomas, G., Yoshimura, A., and Legius, E. (2007) Germline loss-of-function mutations in SPRED1 cause a neurofibromatosis 1–like phenotype. *Nat Genet*. 39, 1120–1126

11. Motta, M., Fasano, G., Gredy, S., Brinkmann, J., Bonnard, A. A., Simsek-Kiper, P. O., Gulec, E. Y., Essaddam, L., Utine, G. E., Prandi, I. G., Venditti, M., Pantaleoni, F., Radio, F. C., Ciolfi, A., Petrini, S., Consoli, F., Vignal, C., Hepbasli, D., Ullrich, M., Boer, E. de, Vissers, L. E. L. M., Gritli, S., Rossi, C., Luca, A. D., Becher, S. B., Gelb, B. D., Dallapiccola, B., Lauri, A., Chillemi, G., Schuh, K., Cavé, H., Zenker, M., and Tartaglia, M. (2021) SPRED2 loss-of-function causes a recessive Noonan syndrome-like phenotype. *Am J Hum Genetics*. 10.1016/j.ajhg.2021.09.007

12. Inoue, H., Kato, R., Fukuyama, S., Nonami, A., Taniguchi, K., Matsumoto, K., Nakano, T., Tsuda, M., Matsumura, M., Kubo, M., Ishikawa, F., Moon, B., Takatsu, K., Nakanishi, Y., and Yoshimura, A. (2005) Spred-1 negatively regulates allergen-induced airway eosinophilia and hyperresponsiveness. *J Exp Med*. 201, 73–82

13. Denayer, E., Ahmed, T., Brems, H., Woerden, G. V., Borgesius, N. Z., Callaerts-Vegh, Z., Yoshimura, A., Hartmann, D., Elgersma, Y., D'Hooge, R., Legius, E., and Balschun, D. (2008) Spred1 Is Required for Synaptic Plasticity and Hippocampus-Dependent Learning. *J Neurosci*. 28, 14443–14449

14. Nobuhisa, I., Kato, R., Inoue, H., Takizawa, M., Okita, K., Yoshimura, A., and Taga, T. (2004) Spred-2 Suppresses Aorta-Gonad-Mesonephros Hematopoiesis by Inhibiting MAP Kinase Activation. *J Exp Medicine*. 199, 737–742

15. Lorenzo, C., and McCormick, F. (2020) SPRED proteins and their roles in signal transduction, development, and malignancy. *Gene Dev*. 34, 1410–1421

16. Freeman, A. K., and Morrison, D. K. (2011) 14-3-3 Proteins: Diverse functions in cell proliferation and cancer progression. *Semin Cell Dev Biol*. 22, 681–687

17. Anjum, R., and Blenis, J. (2008) The RSK family of kinases: emerging roles in cellular signalling. *Nat Rev Mol Cell Bio*. 9, 747–758

18. Carriere, A., Ray, H., Blenis, J., and Roux, P. P. (2008) The RSK factors of activating the Ras/MAPK signaling cascade. *Front Biosci*. Volume, 4258

19. Chrestensen, C. A., and Sturgill, T. W. (2002) Characterization of the p90 Ribosomal S6 Kinase 2 Carboxyl-terminal Domain as a Protein Kinase*. *J Biol Chem*. 277, 27733–27741

20. Pearce, L. R., Komander, D., and Alessi, D. R. (2010) The nuts and bolts of AGC protein kinases. *Nat Rev Mol Cell Bio*. 11, 9–22

21. Samuels, M. L., Weber, M. J., Bishop, J. M., and McMahon, M. (1993) Conditional transformation of cells and rapid activation of the mitogen-activated protein kinase cascade by an estradiol-dependent human raf-1 protein kinase. *Mol Cell Biol*. 13, 6241–6252

22. Boughan, P. K., Argent, R. H., Body-Malapel, M., Park, J.-H., Ewings, K. E., Bowie, A. G., Ong, S. J., Cook, S. J., Sorensen, O. E., Manzo, B. A., Inohara, N., Klein, N. J., Nuñez, G., Atherton, J. C., and Bajaj-Elliott, M. (2006) Nucleotide-binding Oligomerization Domain-1 and Epidermal Growth Factor Receptor CRITICAL REGULATORS OF β-DEFENSINS DURING HELICOBACTER PYLORI INFECTION*. *J Biol Chem*. 281, 11637–11648

23. Sorgeloos, F., Peeters, M., Hayashi, Y., Borghese, F., Capelli, N., Drappier, M., Cesaro, T., Colau, D., Stroobant, V., Vertommen, D., Bodt, G. de, Messe, S., Forné, I., Mueller-Planitz, F., Collet, J.-F., and Michiels, T. (2022) A case of convergent evolution: Several viral and bacterial pathogens hijack RSK kinases through a common linear motif. *P Natl Acad Sci Usa*. 119, e2114647119

24. Cesare, D. D., Jacquot, S., Hanauer, A., and Sassone-Corsi, P. (1998) Rsk-2 activity is necessary for epidermal growth factor-induced phosphorylation of CREB protein and transcription of c-fos gene. *Proc National Acad Sci*. 95, 12202–12207

25. Saha, M., Carriere, A., Cheerathodi, M., Zhang, X., Lavoie, G., Rush, J., Roux, P. P., and Ballif, B. A. (2012) RSK phosphorylates SOS1 creating 14-3-3-docking sites and negatively regulating MAPK activation. *Biochem J*. 447, 159–66

26. Waas, W. F., and Dalby, K. N. (2002) Transient Protein-Protein Interactions and a Random-ordered Kinetic Mechanism for the Phosphorylation of a Transcription Factor by Extracellular-regulated Protein Kinase 2∗. *J Biol Chem*. 277, 12532–12540

27. Wang, Z., and Cole, P. A. (2014) Catalytic mechanisms and regulation of protein kinases. *Methods Enzymol*. 548, 1–21

28. Alexa, A., Sok, P., Gross, F., Albert, K., Kobori, E., Póti, Á. L., Gógl, G., Bento, I., Kuang, E., Taylor, S. S., Zhu, F., Ciliberto, A., and Reményi, A. (2022) A non-catalytic herpesviral protein reconfigures ERK-RSK signaling by targeting kinase docking systems in the host. *Nat Commun*. 13, 472

29. Richards, S. A., Dreisbach, V. C., Murphy, L. O., and Blenis, J. (2001) Characterization of Regulatory Events Associated with Membrane Targeting of p90 Ribosomal S6 Kinase 1. *Mol Cell Biol*. 21, 7470–7480

30. Cheng, D. K., Oni, T. E., Park, Y., Thalappillil, J. S., Ting, H.-C., Alagesan, B., Prasad, N., Rivera, K. D., Pappin, D. J., Aelst, L. V., and Tuveson, D. A. (2020) Oncogenic KRAS engages an RSK1/NF1 complex in pancreatic cancer. *Biorxiv*. 10.1101/2020.09.14.295394

31. Vik, T. A., and Ryder, J. W. (1997) Identification of Serine 380 as the Major Site of Autophosphorylation of Xenopus pp90rsk. *Biochem Bioph Res Co*. 235, 398–402

32. Dalby, K. N., Morrice, N., Caudwell, F. B., Avruch, J., and Cohen, P. (1998) Identification of Regulatory Phosphorylation Sites in Mitogen-activated Protein Kinase (MAPK)-activated Protein Kinase-1a/p90 rsk That Are Inducible by MAPK*. *J Biol Chem*. 273, 1496–1505

33. Trivier, E., Cesare, D. D., Jacquot, S., Pannetier, S., Zackai, E., Young, I., Mandel, J.-L., Sassone-Corsi, P., and Hanauer, A. (1996) Mutations in the kinase Rsk-2 associated with Coffin-Lowry syndrome. *Nature*. 384, 567–570

34. Lv, Y., Zhu, L., Zheng, J., Wu, D., and Shao, J. (2019) Growth Concerns in Coffin–Lowry Syndrome: A Case Report and Literature Review. *Frontiers Pediatrics*. 6, 430

35. Harum, K. H., Alemi, L., and Johnston, M. V. (2001) Cognitive impairment in Coffin-Lowry syndrome correlates with reduced RSK2 activation. *Neurology*. 56, 207–214

36. Hanauer, A., and Young, I. D. (2002) Coffin-Lowry syndrome: clinical and molecular features. *J Med Genet*. 39, 705–713

37. Rauen, K. A. (2013) The RASopathies. *Annu Rev Genom Hum G*. 14, 355–369

38. Cornell, B., and Toyo-oka, K. (2017) 14-3-3 Proteins in Brain Development: Neurogenesis, Neuronal Migration and Neuromorphogenesis. *Front Mol Neurosci*. 10, 318

39. Fellmann, C., Hoffmann, T., Sridhar, V., Hopfgartner, B., Muhar, M., Roth, M., Lai, D. Y., Barbosa, I. A. M., Kwon, J. S., Guan, Y., Sinha, N., and Zuber, J. (2013) An Optimized microRNA Backbone for Effective Single-Copy RNAi. *Cell Reports*. 5, 1704–1713

40. Taylor, T., Denson, J.-P., and Esposito, D. (2017) Optimizing Expression and Solubility of Proteins in E. coli Using Modified Media and Induction Parameters. *Methods Mol Biology Clifton N J*. 1586, 65–82

41. Kopra, K., Vuorinen, E., Abreu-Blanco, M., Wang, Q., Eskonen, V., Gillette, W., Pulliainen, A. T., Holderfield, M., and Härmä, H. (2020) Homogeneous Dual-Parametric-Coupled Assay for Simultaneous Nucleotide Exchange and KRAS/RAF-RBD Interaction Monitoring. *Anal Chem*. 92, 4971–4979

42. Castel, P., Cheng, A., Cuevas-Navarro, A., Everman, D. B., Papageorge, A. G., Simanshu, D. K., Tankka, A., Galeas, J., Urisman, A., and McCormick, F. (2019) RIT1 oncoproteins escape LZTR1-mediated proteolysis. *Science*. 363, 1226–1230

43. Cuevas-Navarro, A., Van, R., Cheng, A., Urisman, A., Castel, P., and McCormick, F. (2021) The RAS GTPase RIT1 compromises mitotic fidelity through spindle assembly checkpoint suppression. *Curr Biol*. 31, 3915-3924.e9

44. Baker, P. R., Trinidad, J. C., and Chalkley, R. J. (2011) Modification Site Localization Scoring Integrated into a Search Engine*. *Mol Cell Proteomics*. 10, M111.008078

45. Chalkley, R. J., and Baker, P. R. (2017) Use of a glycosylation site database to improve glycopeptide identification from complex mixtures. *Anal Bioanal Chem*. 409, 571–577

46. Bateman, A., Martin, M.-J., Orchard, S., Magrane, M., Alpi, E., Bely, B., Bingley, M., Britto, R., Bursteinas, B., Busiello, G., Bye-A-Jee, H., Silva, A. D., Giorgi, M. D., Dogan, T., Castro, L. G., Garmiri, P., Georghiou, G., Gonzales, D., Gonzales, L., Hatton-Ellis, E., Ignatchenko, A., Ishtiaq, R., Jokinen, P., Joshi, V., Jyothi, D., Lopez, R., Luo, J., Lussi, Y., MacDougall, A., Madeira, F., Mahmoudy, M., Menchi, M., Nightingale, A., Onwubiko, J., Palka, B., Pichler, K., Pundir, S., Qi, G., Raj, S., Renaux, A., Lopez, M. R., Saidi, R., Sawford, T., Shypitsyna, A., Speretta, E., Turner, E., Tyagi, N., Vasudev, P., Volynkin, V., Wardell, T., Warner, K., Watkins,

X., Zaru, R., Zellner, H., Bridge, A., Xenarios, I., Poux, S., Redaschi, N., Aimo, L., Argoud-Puy, G., Auchincloss, A., Axelsen, K., Bansal, P., Baratin, D., Blatter, M.-C., Bolleman, J., Boutet, E., Breuza, L., Casals-Casas, C., Castro, E. de, Coudert, E., Cuche, B., Doche, M., Dornevil, D., Estreicher, A., Famiglietti, L., Feuermann, M., Gasteiger, E., Gehant, S., Gerritsen, V., Gos, A., Gruaz, N., Hinz, U., Hulo, C., Hyka-Nouspikel, N., Jungo, F., Keller, G., Kerhornou, A., Lara, V., Lemercier, P., Lieberherr, D., Lombardot, T., Martin, X., Masson, P., Morgat, A., Neto, T. B., Paesano, S., Pedruzzi, I., Pilbout, S., Pozzato, M., Pruess, M., Rivoire, C., Sigrist, C., Sonesson, K., Stutz, A., Sundaram, S., Tognolli, M., Verbregue, L., Wu, C. H., Arighi, C. N., Arminski, L., Chen, C., Chen, Y., Cowart, J., Garavelli, J. S., Huang, H., Laiho, K., McGarvey, P., Natale, D. A., Ross, K., Vinayaka, C. R., Wang, Q., Wang, Y., Yeh, L.-S., and Zhang, J. (2019) UniProt: a worldwide hub of protein knowledge. *Nucleic Acids Res*. 47, D506–D515

47. Pino, L. K., Searle, B. C., Bollinger, J. G., Nunn, B., MacLean, B., and MacCoss, M. J. (2020) The Skyline ecosystem: Informatics for quantitative mass spectrometry proteomics. *Mass Spectrom Rev*. 39, 229–244

48. Choi, M., Chang, C.-Y., Clough, T., Broudy, D., Killeen, T., MacLean, B., and Vitek, O. (2014) MSstats: an R package for statistical analysis of quantitative mass spectrometry-based proteomic experiments. *Bioinformatics*. 30, 2524–2526

49. Kabsch, W. (2010) XDS. *Acta Crystallogr Sect D Biological Crystallogr*. 66, 125–132

50. Winn, M. D., Ballard, C. C., Cowtan, K. D., Dodson, E. J., Emsley, P., Evans, P. R., Keegan, R. M., Krissinel, E. B., Leslie, A. G. W., McCoy, A., McNicholas, S. J., Murshudov, G. N., Pannu, N. S., Potterton, E. A., Powell, H. R., Read, R. J., Vagin, A., and Wilson, K. S. (2011)

Overview of the CCP4 suite and current developments. *Acta Crystallogr Sect D Biological Crystallogr*. 67, 235–242

51. Murshudov, G. N., Skubák, P., Lebedev, A. A., Pannu, N. S., Steiner, R. A., Nicholls, R. A., Winn, M. D., Long, F., and Vagin, A. A. (2011) REFMAC5 for the refinement of macromolecular crystal structures. *Acta Crystallogr Sect D Biological Crystallogr*. 67, 355–367

52. Emsley, P., Lohkamp, B., Scott, W. G., and Cowtan, K. (2010) Features and development of Coot. *Acta Crystallogr Sect D Biological Crystallogr*. 66, 486–501

53. Liebschner, D., Afonine, P. V., Baker, M. L., Bunkóczi, G., Chen, V. B., Croll, T. I., Hintze, B., Hung, L.-W., Jain, S., McCoy, A. J., Moriarty, N. W., Oeffner, R. D., Poon, B. K., Prisant, M. G., Read, R. J., Richardson, J. S., Richardson, D. C., Sammito, M. D., Sobolev, O. V., Stockwell, D. H., Terwilliger, T. C., Urzhumtsev, A. G., Videau, L. L., Williams, C. J., and Adams, P. D. (2019) Macromolecular structure determination using X-rays, neutrons and electrons: recent developments in Phenix. *Acta Crystallogr Sect D*. 75, 861–877

54. Morin, A., Eisenbraun, B., Key, J., Sanschagrin, P. C., Timony, M. A., Ottaviano, M., and Sliz, P. (2013) Collaboration gets the most out of software. *Elife*. 2, e01456

Chapter 3: Lack of Noonan syndrome-like phenotype in Spred2 knockout mice

We read with interest the manuscript by Motta *et al*, describing *SPRED2* loss-of-function mutations in individuals with a Noonan syndrome (NS)-like phenotype. NS is a neurodevelopmental disorder caused by autosomal dominant or recessive mutations in the genes encoding for key components and/or regulators of the RAS-MAPK pathway, including *PTPN11*, *RAF1*, *SOS1*, *RIT1*, *LZTR1*, *KRAS* and others (1). Motta *et al* demonstrate that *SPRED2* deletion in cells leads to hyperactive MAPK signaling in response to growth factors, a pathognomonic finding in NS. In addition, the authors use *Spred2* knockout mice to support their claim that loss of *Spred2* causes a NS-like phenotype. Mice have been previously shown to be an excellent organism to model Noonan syndrome and several compound mutant mice have been described, including the most frequent NS genotypes *Ptpn11*, *Raf1*, and *Rit1* (2-4). In mice, NS-like phenotypes are characterized by dysmorphic skull features (round skull, blunt snout, hypertelorism), small size at early ages, and increased heart and spleen size, among others (5). Consistently, Motta *et al* report that *Spred2* knockout mice exhibit cardiac defects, skeletal abnormalities, growth abnormalities, phenocopying common attributes found in NS patients. We, however, report major discrepancies in the mouse phenotypes published in this article using our *Spred2* knockout allele.

NS patients are characterized by various skeletal malformations including craniofacial abnormalities and short stature (6). Motta et al. report the skeletal defects of scoliosis, growth retardation, and reduction of skull length in *Spred2* knockout mice. In our studies, we extensively monitored the skull phenotypes of *Spred2* knockout mice using computed tomography (CT) and did not detect any significant differences when compared to wild type (WT) littermates at 8 weeks of age (**Figure 3.1B**, **supplemental 3.1B)**. We also did not detect significant differences in the

skull length and intercanthal distance in 16-week-old mice. Given that heart defects are another clinical feature of NS, we also performed echocardiography and measured the heart weight-to-body weight ratios in *Spred2* knockout mice; our data did not reveal any significant differences compared to WT littermates (**Figure 3.1C, supplemental 3.1B**). In further analysis, we did not detect any differences in the weight of mice over 8 weeks and in weight-to-body weight ratios of the spleen, pancreas, and kidney (**Figure 3.1D, supplemental 3.1D**). Additionally, we observed no functional differences in p-ERK levels in Mouse Embryonic Fibroblasts (MEFs) generated from *Spred2* WT and KO mice when serum starved and stimulated with epidermal growth factor (**Figure 3.1E)**. Overall, our data shows no statistically significant differences between *Spred2* WT and knockout mice in any of the NS-like phenotypes monitored and, therefore, we conclude that our *Spred2* knockout mice do not phenocopy NS nor are a reliable mouse model of NS.

We reason that the discrepancy in data from Motta *et al* could be explained by the different origin of *Spred2* knockout mice. The mice described by Motta *et al* were generated using the mouse embryonic stem cells from the gene trap mutagenesis project developed by BayGenomics, while our mice were generated using CRISPR/Cas9 as part of the Knockout Mouse Project and could be obtained from the Mutant Mouse Resource & Research Centers (7, 8). Comparatively, the exon gene trap method can be less specific and has been previously reported to result in hypomorphic alleles (9). Additionally, we noticed that the gene trap is inserted between *Spred2* exons 4 and 5, which potentially results in the expression of a functional N-terminal protein domain (EVH1) fused to the B-geo reporter (**Figure 3.1F**). Given that the Spred2 EVH1 domain displays a high level of conservation with Spred1/3 and is required for its association with neurofibromin, the resulting chimeric protein could act as a dominant negative in these mice, inhibiting all Spred proteins, and leading to multiple effects that explain the inconsistency in phenotypes reported by Motta *et al*. In

contrast, in our *Spred2* knockout mice, exon 2 (containing the initiating codon) and the flanking splicing regions were constitutively deleted; as a result, we do not detect Spred2 protein in the knockout mice. Additionally, we note differences in the background of the *Spred2* mice. Motta *et al* use a mixed background to generate their *Spred2* knockout mice while we use a pure C57BL/6N background. It has been previously reported that the NS phenotypes observed in mice are dependent on the genetic background, and C57BL/6 has also been reported to be more sensitive to these phenotypes (10).

In light of the emerging clinical relevance of *SPRED2* loss-of-function in humans, we find that it is important to accurately characterize *Spred2* knockout mice and clarify the conflicting phenotypes of the different *Spred2* mutant alleles.

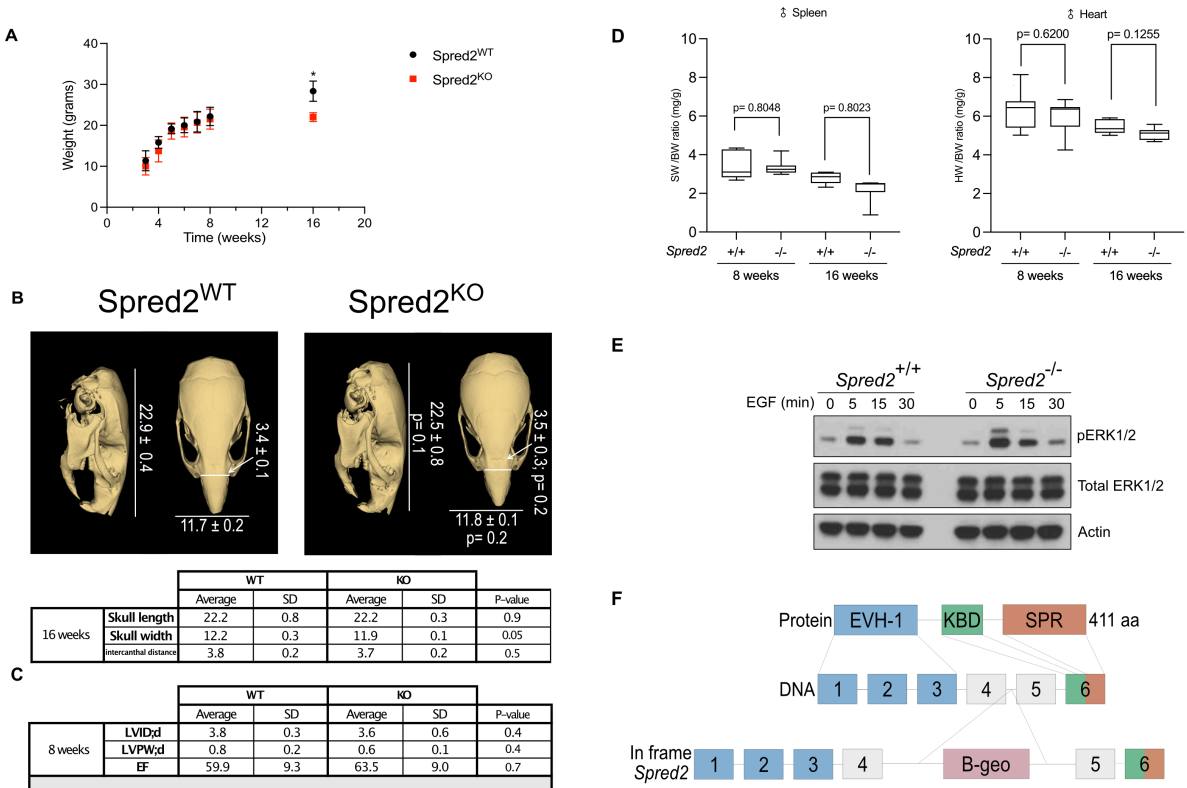

		WT		KO		
		Average	SD	Average	SD	P-value
16 weeks	Skull length	22.2	0.8	22.2	0.3	0.9
	Skull width	12.2	0.3	11.9	0.1	0.05
	Intercanthal distance	3.8	0.2	3.7	0.2	0.5

C

		WT		KO		
		Average	SD	Average	SD	P-value
8 weeks	LVID;d	3.8	0.3	3.6	0.6	0.4
	LVPW;d	0.8	0.2	0.6	0.1	0.4
	EF	59.9	9.3	63.5	9.0	0.7
16 weeks	LVID;d	3.7	0.3	3.9	0.2	0.4
	LVPW;d	0.8	0.1	0.7	0.05	0.03
	EF	48.3	7.3	60.6	5.8	0.1

Figure 3.1: Analysis of *Spred2* mice phenotype

A, Analysis of male *Spred2* KO mice and WT littermate weight. ***B,*** Micro computed tomography (µCT) analysis of male *Spred2* KO mice and WT littermates. The values are average measurements (mm) and the standard deviation of the length, width, and inner intercanthal distance at 8 weeks (WT, n= 7; KO, n= 7). Average measurements at 16 weeks are represented in the table (WT, n= 5; KO, n= 6) . The *P* values were calculated by using the Mann-Whitney test. ***C***, Echocardiography of *Spred2* KO mice and WT littermates in 8- and 16-week-old littermates. ***D***, Quantification of spleen and heart weight- to body ratios in 8- and 16-week-old littermates. ***E***, Immunoblots of phosphorylated ERK in *Spred2* WT and KO Mouse Embryonic Fibroblasts (MEFs) deprived of serum for 18 hours and then stimulated with epidermal growth factor (EGF, 20ng/mL) for indicated times. ***E***, Model of genetrap insertion in *Spred2* mice.

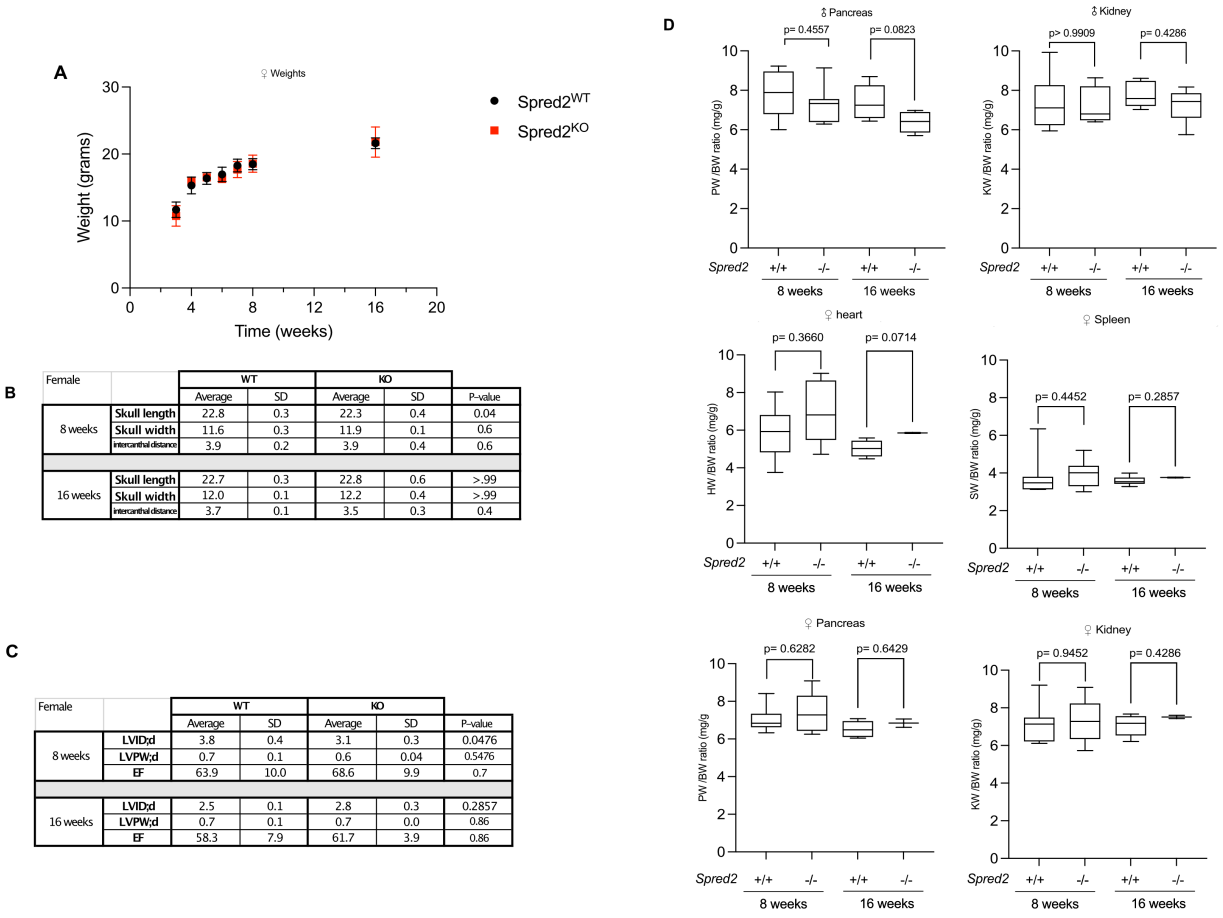

B

Female		WT		KO		
		Average	SD	Average	SD	P-value
8 weeks	Skull length	22.8	0.3	22.3	0.4	0.04
	Skull width	11.6	0.3	11.9	0.1	0.6
	Intercanthal distance	3.9	0.2	3.9	0.4	0.6
16 weeks	Skull length	22.7	0.3	22.8	0.6	>.99
	Skull width	12.0	0.1	12.2	0.4	>.99
	Intercanthal distance	3.7	0.1	3.5	0.3	0.4

C

Female		WT		KO		
		Average	SD	Average	SD	P-value
8 weeks	LVIDd	3.8	0.4	3.1	0.3	0.0476
	LVPWd	0.7	0.1	0.6	0.04	0.5476
	EF	63.9	10.0	68.6	9.9	0.7
16 weeks	LVIDd	2.5	0.1	2.8	0.3	0.2857
	LVPWd	0.7	0.1	0.7	0.0	0.86
	EF	58.3	7.9	61.7	3.9	0.86

Supplementary Figure 3.1: Analysis of *Spred2* mice phenotype

A, Analysis of female *Spred2* KO mice and WT littermate weight. ***B***, Micro computed tomography (µCT) analysis of female *Spred2* KO mice and WT littermates. The values are average measurements (mm) and the standard deviation of the length, width, and inner intercanthal distance at 8 and 16 weeks. The *P* values were calculated by using the Mann-Whitney test. ***C***, Echocardiography of female *Spred2* KO mice and WT littermates in 8- and 16-week-old littermates. ***D***, Quantification of male pancreas and kidney in 8- and 16-week-old littermates and female heart, spleen, pancreas, and kidney weight- to body ratios in 8- and 16-week-old littermates.

References:

1. Rauen, K. A. (2012) The RASopathies. *Genom Hum Genetics*. 14, 355–369

2. Hernández-Porras, I., Fabbiano, S., Schuhmacher, A. J., Aicher, A., Cañamero, M., Cámara, J. A., Cussó, L., Desco, M., Heeschen, C., Mulero, F., Bustelo, X. R., Guerra, C., and Barbacid, M. (2014) K-RasV14I recapitulates Noonan syndrome in mice. *Proc National Acad Sci*. 111, 16395–16400

3. Castel, P., Cheng, A., Cuevas-Navarro, A., Everman, D. B., Papageorge, A. G., Simanshu, D. K., Tankka, A., Galeas, J., Urisman, A., and McCormick, F. (2019) RIT1 oncoproteins escape LZTR1-mediated proteolysis. *Science*. 363, 1226–1230

4. Wu, X., Simpson, J., Hong, J. H., Kim, K.-H., Thavarajah, N. K., Backx, P. H., Neel, B. G., and Araki, T. (2011) MEK-ERK pathway modulation ameliorates disease phenotypes in a mouse model of Noonan syndrome associated with the Raf1L613V mutation. *J Clin Invest*. 121, 1009–1025

5. Schuhmacher, A. J., Hernández-Porras, I., García-Medina, R., and Guerra, C. (2017) Noonan syndrome: lessons learned from genetically modified mouse models. *Expert Rev Endocrinol Metabolism*. 12, 367–378

6. Roberts, A. E., Allanson, J. E., Tartaglia, M., and Gelb, B. D. (2013) Noonan syndrome. *Lancet*. 381, 333–342

7. Stryke, D., Kawamoto, M., Huang, C. C., Johns, S. J., King, L. A., Harper, C. A., Meng, E. C., Lee, R. E., Yee, A., L'Italien, L., Chuang, P.-T., Young, S. G., Skarnes, W. C., Babbitt, P. C.,

and Ferrin, T. E. (2003) BayGenomics: a resource of insertional mutations in mouse embryonic stem cells. *Nucleic Acids Res*. 31, 278–281

8. Austin, C. P., Battey, J. F., Bradley, A., Bucan, M., Capecchi, M., Collins, F. S., Dove, W. F., Duyk, G., Dymecki, S., Eppig, J. T., Grieder, F. B., Heintz, N., Hicks, G., Insel, T. R., Joyner, A., Koller, B. H., Lloyd, K. C. K., Magnuson, T., Moore, M. W., Nagy, A., Pollock, J. D., Roses, A. D., Sands, A. T., Seed, B., Skarnes, W. C., Snoddy, J., Soriano, P., Stewart, D. J., Stewart, F., Stillman, B., Varmus, H., Varticovski, L., Verma, I. M., Vogt, T. F., Melchner, H. von, Witkowski, J., Woychik, R. P., Wurst, W., Yancopoulos, G. D., Young, S. G., and Zambrowicz, B. (2004) The Knockout Mouse Project. *Nat Genet*. 36, 921–924

9. Raymond, C. S., and Soriano, P. (2006) Engineering mutations: Deconstructing the mouse gene by gene. *Dev. Dyn.* 235, 2424–2436

10. Hernández-Porras, I., Jiménez-Catalán, B., Schuhmacher, A. J., and Guerra, C. (2015) The impact of the genetic background in the Noonan syndrome phenotype induced by K-RasV14I. *Rare Dis*. 3, e1045169

Publishing Agreement

It is the policy of the University to encourage open access and broad distribution of all theses, dissertations, and manuscripts. The Graduate Division will facilitate the distribution of UCSF theses, dissertations, and manuscripts to the UCSF Library for open access and distribution. UCSF will make such theses, dissertations, and manuscripts accessible to the public and will take reasonable steps to preserve these works in perpetuity.

I hereby grant the non-exclusive, perpetual right to The Regents of the University of California to reproduce, publicly display, distribute, preserve, and publish copies of my thesis, dissertation, or manuscript in any form or media, now existing or later derived, including access online for teaching, research, and public service purposes.

DocuSigned by:
Jocelyne Lopez
D4BAA347EC8443B...
Author Signature

5/13/2023
Date